Discovery of an endoplasmic reticulum proteostasis modulator that enhances insulin production in pancreatic β cells

Masato Miyake[1, 2, 3, 10]*, Mitsuaki Sobajima[1, 2], Kiyoe Kurahashi[1, 2, 4], Akira Shigenaga[5, 6], Masaya Denda[5], Akira Otaka[5], Tomohide Saio[7, 8], Naoki Sakane[9], Hidetaka Kosako[3], and Seiichi Oyadomari[1, 2, 3]*

Affiliations

[1]Division of Molecular Biology, Institute of Advanced Medical Sciences, Tokushima University, Tokushima, Japan

[2]Department of Molecular Research, Diabetes Therapeutics and Research Center, Tokushima University, Tokushima, Japan

[3]Fujii Memorial Institute of Medical Sciences, Institute of Advanced Medical Sciences, Tokushima University, Tokushima, Japan.

[4]Department of Hematology, Endocrinology and Metabolism, Graduate School of Biomedical Sciences, Tokushima University, Tokushima, Japan

[5]Institute of Biomedical Sciences and Graduate School of Pharmaceutical Sciences, Tokushima University, Tokushima, Japan.

[6]Faculty of Pharmacy and Pharmaceutical Sciences, Fukuyama University, Hiroshima, Japan

[7]Division of Molecular Life Science, Institute of Advanced Medical Sciences, Tokushima University, Tokushima, Japan

[8]Department of Chemistry, Faculty of Science, Hokkaido University, Sapporo, Hokkaido, Japan.

[9]Pharmaceutical Frontier Research Laboratories, JT Inc., Yokohama, Japan

[10]Lead Contact

*Corresponding authors

Masato Miyake: miyake@genome.tokushima-u.ac.jp

Seiichi Oyadomari: oyadomar@genome.tokushima-u.ac.jp

Summary

Perturbation of endoplasmic reticulum (ER) proteostasis is associated with impairment of cellular function in diverse diseases, especially the function of pancreatic β cells in type 2 diabetes. Restoration of ER proteostasis by small molecules thus shows therapeutic promise for type 2 diabetes. Here, we report the discovery of a new chemical chaperone-like small molecule, KM04794, that alleviates ER stress using cell-based screening. KM04794 prevented protein aggregation and cell death caused by ER stressors and a mutant insulin protein. We also found that this compound increased intracellular and secreted insulin levels in pancreatic β cells. Chemical biology and biochemical approaches revealed that the compound accumulated in the ER and directly interacted with the ER molecular chaperone BiP. Our data show that this new corrector of ER proteostasis can enhance insulin storage and pancreatic β cell function.

Keywords

ER stress, unfolded protein response, pancreatic β cell, insulin, chemical chaperone, BiP

Introduction

Protein homeostasis (proteostasis) in the endoplasmic reticulum (ER) is maintained through the functions of molecular chaperones to assist protein folding and prevent aggregation. The accumulation of misfolded or aggregated proteins in the ER beyond the ability of molecular chaperones leads to ER stress and activates adaptive stress-responsive signaling in a process called the unfolded protein response (UPR) in eukaryotic cells (Han and Kaufman, 2017; Mori, 2000; Walter and Ron, 2011). The UPR coordinates ER homeostasis through transcriptional and translational regulation initiated by three ER transmembrane proteins, IRE1, PERK and ATF6, which act as sensors of unfolded protein accumulation and transducers of the UPR. Downstream transcription factors, such as XBP1, ATF4 and a truncated form of ATF6, induce the expression of ER molecular chaperones and ER folding enzymes, such as the abundant ER molecular chaperone BiP. Excessive ER stress and dysregulation of the UPR are known to be related to the pathology of various types of diseases, including diabetes, neurodegenerative disorders and cancers (Clarke et al., 2014; Hotamisligil, 2010; Martínez et al., 2018).

Accumulated evidence suggests a relationship between ER proteostasis and the pathogenesis of type 2 diabetes. In particular, the function and survival of pancreatic β cells are closely related to ER stress and the UPR (Fonseca et al., 2011; Rabhi et al., 2014). The hypersynthesis of insulin to compensate for insulin resistance in type 2 diabetes increases the ER burden and insulin misfolding and causes ER stress, leading to loss of function and survival in pancreatic β cells (Arunagiri et al., 2018; Back and Kaufman, 2012; Eizirik and Cnop, 2010). UPR signaling components are essential for the maintenance and function of pancreatic β cells (Harding et al., 2001; Hassler et al., 2015; Lee et al., 2011; Tsuchiya et al., 2018; Zhang et al., 2006). Molecular chaperones and folding enzymes, such as BiP, GRP94, and ERO1β, support proper insulin folding and insulin secretion in mouse pancreatic β cells (Ghiasi et al., 2019; Zhang et al., 2009; Zito et al., 2010). Studies using *Akita* mice, in which the cysteine in the 96th position of insulin is mutated to tyrosine, have shown the importance of insulin synthesis and folding homeostasis since *Akita* mice develop severe diabetes due to pancreatic β cell death induced by insulin misfolding (Oyadomari et al., 2002; Wang et al., 1999). These data indicate that the improvement of ER proteostasis in pancreatic β cells is a promising approach for treating type 2 diabetes.

Several small molecules that modulate ER stress and the UPR to improve diabetes have been identified and applied to mouse disease models and human patients. For example, the classical chemical chaperone 4-phenylbutyrate (4PBA) and tauroursodeoxycholic acid (TUDCA) alleviated diabetes in mice and humans (Ozcan et al., 2006; Xiao et al., 2011). Fu et al. discovered that azoramide modulates the UPR and has antidiabetic activity in a phenotypic screen (Fu et al., 2015). In pancreatic β cells, γ-orizanol and compound 13d were reported to decrease pancreatic β cell death due to a reduction in ER stress in mice (Duan et al., 2017; Kozuka et al., 2015). Antioxidants function to maintain pancreatic β cell function (Han et al., 2015). As a pathway-specific modulator of the UPR, an allosteric inhibitor of the RNase IRE1, KIRA6, reduced β cell apoptosis in the diabetic *Akita* mouse model (Ghosh et al., 2014). However, few small molecules that improve ER proteostasis and insulin secretion in pancreatic β cells have been identified despite their importance shown by basic research.

Some screening systems have been developed to identify chemical chaperones or UPR modulators (Grandjean and Wiseman, 2020). Here, we conducted small-molecule screening through the utilization of a transcription factor-binding element; this assay system enabled us to find specific signaling modulators or general modulators of ER homeostasis. We discovered one small molecule that strongly reduced ER stress and increased intracellular insulin in pancreatic β cells. Chemical biology and biochemical approaches revealed that the molecular chaperone BiP at least partially mediates the effects of the small molecule. Our findings reveal a new type of chemical chaperone-like small molecule for pancreatic β cells.

Results

Cell-based screening for UPR signaling molecules identified the inhibitory compound KM04794

The three branches of the UPR activate transcription via regulation by the transcription factors XBP1, ATF4 and ATF6. The main XBP1-, ATF4- and ATF6-binding sequences are the UPRE (Yoshida et al., 2001), AARE (Bruhat et al., 2000) and ERSE (Yoshida et al., 1998), respectively (Figure 1A). To identify modulators of the UPR, we established three independent reporter cell lines expressing luciferase under the control of the UPRE using C2C12 myoblast cells (C2C12:UPRE), under the control of the ERSE using C2C12 myoblast cells (C2C12:ERSE) and under the control of the AARE using MIN6m9 pancreatic β cells (MIN6:AARE). The ER stressor tunicamycin (Tm), an inhibitor of N-linked glycosylation, induced a 3- to 5-fold increase in luciferase activity in each cell line (Figure 1B, C and D). Specific inhibitors of each branch (4u8c for IRE1-XBP1, the S1P inhibitor PF-429242 for ATF6 and the PERK inhibitor GSK2606414 for PERK-ATF4) completely suppressed luciferase activation in each cell line (Figure 1B, C and D). Therefore, these cell lines could be used to separately monitor the activation of each UPR pathway. Previously, we identified AARE-activating compounds from among 4,000 compounds using C2C12 myoblast cells expressing AARE-luciferase (Miyake et al., 2016). We tested the effects of these hit compounds on Tm-induced luciferase activity in these three newly established reporter cell lines (C2C12:UPRE, C2C12:ERSE, and MIN6m9:AARE) and discovered that N'1-[3-(trifluoromethyl)benzoyl]-2-{2-[(4-chlorobenzyl)thio]phenoxy}ethanohydrazide inhibited Tm-induced luciferase reporter activity in all cell lines (Figure 1E). We named the compound identified in this study KM04794. The 50% inhibitory concentration (IC50) was determined to be 9.3 μM, 9.9 μM and 16.0 μM in the UPRE, ERSE, and AARE cell lines (Figure 1F, G and H). KM04794 did not show cellular toxicity until 30 μM over 12 h of treatment (Figure S1A). To confirm the effect of KM04794 on the UPR, we used another CHO cell-derived reporter cell line that expressed GFP controlled by the CHOP promoter. KM04794 also inhibited CHOP reporter activity, as monitored by fluorescence-activated cell sorting (FACS) (Figure S1B).

KM04794 inhibited UPR activation by ER stressors

The inhibitory effects of KM04794 on reporter activation by Tm were continued for 18 h in the C2C12:UPRE and MIN6:AARE reporter cell lines (Figure 2A and 2B). In addition to Tm-induced ER stress, we examined the effects of KM04794 on thapsigargin (Tg) and dithiothreitol (DTT), which are also ER stressors, in the C2C12:UPRE and MIN6:AARE reporter cell lines at several time points. These compounds are believed to cause ER stress more rapidly than Tm in cells pretreated with KM04794. KM04794 significantly inhibited luciferase activity induced by Tg in both reporter cell lines (Figure 2C and D). The inhibitory effects of KM04794 were significant at 12 h but weak against DTT-induced reporter activation in C2C12:UPRE cells (Figure S2A). The effects of KM04794 on DTT could not be measured in MIN6m9:AARE cells due to rapid cell death (data not shown). To exclude pseudoinhibition of luciferase activity independent of the UPR, UPR signaling was examined by immunoblotting and RT-qPCR analysis in the MIN6m9 pancreatic β cell line. KM04794 suppressed the Tm-induced phosphorylation of IRE1 and PERK and induction of XBP1 and ATF4 (Figures 2E and S2B). Cleavage of ATF6 was also suppressed by KM04794 (Figures 2E and S2B). The inhibition of eIF2α phosphorylation may have been nonsignificant due to the timing of its detection. The immunoblot analysis also showed that the activation of the UPR induced by brefeldin A (Bre), which is another stressor, was suppressed by KM04794 (Figure 2E and S2C). The mRNA expression levels of target genes in each branch of the UPR (spliced *Xbp1* in the IRE1 branch, *BiP* in all branches, *Chop* and *Atf3* in the PERK branch and *Herpud1* in the ATF6 branch) were induced by Tm and Bre and were almost downregulated by cotreatment with KM04794 from 6 to 24 h (Figure 2F and 2G). KM04794 inhibited UPR signaling in not only MIN6m9 cells but also mouse embryonic fibroblasts (MEFs) for 12 h (Figure S2D). The inhibitory effects of KM04794 seemed to be stronger than those of the known chemical chaperones 4PBA and TUDCA, at least when the level of UPR signaling activation was measured (Figure S2E). These data confirmed the inhibitory effects of KM04794 on UPR signaling.

ER protein aggregation and ER stress-induced cell death were alleviated by KM04794

Since KM04794 inhibited all UPR signaling branches, ER stress may be alleviated by KM04794. Evaluation of total translation by [35S]Met/Cys labeling showed it to be equivalent in DMSO- and KM04794-treated cells (Figure 3A), indicating that new protein synthesis in the ER was not affected by

KM04794. Next, we measured the amount of Tm-induced protein aggregate complexes containing the ER chaperone BiP bound to misfolded proteins in MEFs (Marciniak et al., 2004). KM04794 dramatically reduced the amount of BiP in the protein aggregates, indicating reductions in misfolded protein aggregation and ER stress (Figure 3B). Accordingly, the cell viability in MEFs after Tm challenge was improved by KM04794 (Figure 3C). The effect of KM04794 on cell viability was stronger than that of 4PBA (Figure 3C). In MIN6m9 cells, the Tm-induced loss of cell viability was blocked by KM04794 (Fig. 3D). These results support the notion that KM04794 alleviates ER stress but does not inhibit UPR signaling and has chaperone-like activity against ER proteins.

KM04794 alleviated mutant insulin-induced ER stress

Genetic mutation of proteins synthesized in the ER often leads to impairment of their proper folding and causes ER stress. The *Ins2* gene mutation in *Akita* mice is one such example. A pancreatic β cell line that expresses *Akita* mutant insulin was found to undergo ER stress, and this cell line is thus useful for examining the effects on ER stress of a proteotoxin rather than other chemical ER stressors (Cunningham et al., 2019; Hartley et al., 2010; Nozaki et al., 2004). We first used an immortalized pancreatic β cell line derived from *Akita* mice to examine the effects of KM04794. UPR target genes were downregulated by treatment with KM04794 in *Akita* β cells, indicating reduced ER stress (Figure 4A). We next developed wild-type MIN6m9 cells with doxycycline-induced expression of *Akita* mutant insulin. As a control, wild-type MIN6m9 cells with doxycycline-induced exogeneous expression of wild-type insulin were prepared simultaneously. Since the overexpression of *Akita* mutant insulin upregulated UPR target genes, the system successfully recapitulates ER stress (Figure 4B). The overexpression of wild-type insulin did not cause ER stress, at least in this system (Fig. S3A). In accordance with the *Akita* mutant cell line, treatment with KM04794 inhibited UPR gene expression (Figure 4B). *Akita* mutant insulin was reported to entrap wild-type proinsulin and form a high-molecular-weight (HMW) insulin complex as shown by SDS-PAGE under nonreducing conditions. The anti-insulin antibody used in this study could not distinguish between endogenous wild-type and exogenous *Akita* mutant insulin, because both wild-type and *Akita* insulin could be detected by IB in each insulin-overexpressed HEK293 cell that does not express insulin endogenously (Fig. S3B). However, overexpression of *Akita* mutant insulin increased

middle-molecular-weight (MMW) and HMW insulin content and decreased the monomeric insulin content in MIN6m9 cells (Figure 4C). The addition of KM04794 reduced MMW and HMW insulin levels and restored monomeric insulin levels (Figure 4C). These data suggest that KM04794 prevents insulin aggregation triggered by the *Akita* mutation.

Intracellular and secreted insulin was increased by KM04794

Since several studies have shown the importance of ER proteostasis in insulin synthesis and secretion in pancreatic β cells, we investigated the function of KM04794 in insulin turnover. Treatment with KM04794 led to a dramatic increase in the medium insulin concentration under both low- and high-glucose conditions in MIN6m9 cells (Figure 5A). Surprisingly, KM04794 also increased the intracellular insulin content (Figure 5B). Thus, the medium insulin per total insulin content was the same with KM04794 and vehicle control treatment, suggesting an increase in insulin biosynthesis but not its secretion under basal conditions (Figure 5C). The effect of KM04794 on insulin biosynthesis required a dose of more than 20 μM in MIN6m9 cells (Figure S4A). Insulin secretion under high-glucose conditions and the insulin content were also increased by treatment with KM04794 in primary mouse pancreatic islets despite similar levels of insulin secretion under low-glucose conditions in cells treated with vehicle and KM04794 (Figure 5D, E). The other typical chemical chaperones 4PBA and TUDCA had no effect on the intracellular insulin content, indicating that the mechanism underlying KM04794's effects on ER homeostasis probably differs from that of these chemical chaperones (Figure S4B). IBT21, which was previously identified as a chemical chaperone, also had no effects on insulin secretion and content (Kitakaze et al., 2019)(Figure S4C). We next examined which step in insulin biosynthesis is important for the upregulation of insulin by KM04794. The mRNA expression level of *Ins2*, the main isoform of insulin in mice, was not changed by KM04794 (Figure S4E). Consistent with this, cotreatment with KM04794 and the transcriptional inhibitor actinomycin D did not abolish induction of the insulin protein (Figure S4F). A cycloheximide (CHX) chase experiment showed that the insulin level was higher in KM04794-treated cells than in vehicle-treated cells at 60 min after the addition of CHX, suggesting that KM04794-induced inhibition of insulin degradation is important for insulin induction (Figure 5F). Excessive ER stress is known to disturb glucose-stimulated insulin secretion in pancreatic β cells. Indeed,

the ER stressor Tm decreased insulin secretion, but KM04794 restored insulin secretion (Figure 5G). Since increased insulin synthesis and ER stress may lead to the secretion of misfolded insulin, we tested whether insulin secreted by KM04794 is active but not misfolded. First, the secreted mature insulin and less active proinsulin were measured in MIN6m9 cells treated with KM04794. KM04794 induced both mature insulin and proinsulin production (Figure 5H, S4G). Tm inhibited the secretion of mature insulin, and KM04794 restored its secretion (Figure 5H, S4G). The ratio of secreted proinsulin molecule per mature insulin molecule was improved by KM04794 compared with Tm (Figure S4H). Next, we analyzed the activity of insulin in medium from MIN6m9 cells. Conditioned medium (CM) was collected from MIN6m9 cells treated with each compound, and insulin-responsive 3T3L1 cells were cultured with the collected CM. Then, the activation of insulin signaling in these 3T3L1 cells was analyzed by evaluating the phosphorylation of Akt (Figure 5I). Tm-treated 3T3L1 cells cultured in CM exhibited lower phosphorylation of Akt than those cultured in control CM, and the Tm-treated cells treated with both KM04794 and CM exhibited restored phosphorylation of Akt (Figure 5I). These two experiments indicate that KM04794 induced the secretion of folded and active insulin. The effect of KM04794 in restoring insulin secretion was also observed in cells overexpressing *Akita* mutant insulin (Figure 5J). These results showed that KM04794 increased intracellular insulin under normal conditions and improved insulin secretion under ER stress conditions.

The effects of KM04794 are mediated in part by its direct binding to BiP

To reveal the molecular mechanism and direct target of KM04794, we used photoaffinity crosslinking and click chemistry to pull down potential KM04794-binding partners. We synthesized a derivative of KM04794 (KM04794-probe) containing benzophenone for the photoactivated covalent attachment of partner proteins and azide for copper-catalyzed azide-alkyne cycloaddition to additionally attach biotin (Figure 6A). In brief, live MIN6m9 cells or MEFs were treated with KM04794-probe and exposed to UV light to attach KM04794-binding proteins to KM04794-probe. After the cells had been lysed, the samples were subjected to biotin conjugation through a click reaction and pulled down using streptavidin for mass spectrometry (Figure 6A). Free KM04794 was used as a competitor for the identification of specific binding proteins. The effect of KM04794-probe on ER stress was the same as that of KM04794

(Figure 6B, S5A and S5B). SDS-PAGE and silver staining analysis showed several specific binding proteins (Figure S5C). We defined a specific KM04794-probe-binding protein based on the following criteria: 1) higher than 5-fold enrichment in samples containing KM04794-probe compared to samples containing KM04794, 2) higher than 1.5-fold enrichment in samples containing KM04794-probe compared to samples cotreated with KM04794, and 3) identified in both MIN6m9 cells and MEFs (Figures 6C and 6D and Table S1). Gene Ontology (GO) enrichment analysis of the identified proteins revealed the enrichment of membrane- and ER-related proteins (Figures 6C and S4C). This result indicates that KM04794 accumulates in the ER. Since KM04794 had effects on ER stress and insulin synthesis and accumulated in ER, the molecular mediator of KM04794's effects is probably localized in the ER and has a related function in ER proteostasis. Thus, we selected 21 genes that met our criteria, as follows (Table S1): 1) classified as a GO:0005783:endoplasmic reticulum cellular component or known as a vesicle trafficking component and 2) not a metabolic enzyme. These genes were knocked down in MIN6m9 cells using a CRISPRi system, and the effect of KM04794 on insulin induction was analyzed. The knockdown of each gene was successful, and only BiP knockdown decreased the insulin contents in MIN6m9 cells (Figure S6A). Therefore, we focused on BiP as a binding partner of KM04794. The pulldown and immunoblot analyses confirmed the binding of KM04794 to BiP (Figure 7A). Although we attempted to show the complete loss of KM04794's effects in BiP-knockout MIN6m9 cells, knockout of BiP led to strong UPR induction, cell death and impaired insulin secretion in the cells (Figure S6B and data not shown). In BiP-knockout cells, we found no effects of KM04794 on the expression levels of UPR genes (Figure S6B). Therefore, we used a CRISPRi system and achieved the moderate knockdown used above. With the CRISPRi system, the expression of BiP mRNA was decreased to half that in the control cells (Figure 7B). The increase in insulin secretion by KM04794 in the control cells was lost in the BiP-knockdown cells (Figure 7C). These results suggest that an adequate expression of BiP is required for the upregulation of insulin in cells. In accordance with the requirement of BiP for insulin induction, KM04794 did not stabilize insulin in BiP knockdown cells during the CHX chase assay, although BiP knockdown led to decreased degradation of insulin (Figure 7D). BiP transiently interacts with substrates in the ER to fold target proteins. Therefore, we analyzed the interaction between BiP and insulin in MIN6m9 cells. Unexpectedly, KM04794 led to a decreased interaction between BiP and insulin

(Figure 7E and S6C). To assess how KM04794 regulates the function of BiP, we analyzed the effects of KM04794 on BiP function *in vitro* using recombinant BiP (Figure S6D). We confirmed that KM04794-probe also bound recombinant mouse BiP (Figure S6E). Monitoring the aggregation of denatured GAPDH showed that KM04794 inhibited the aggregation of GAPDH in cooperation with BiP (Figure 7F). Although ATPase activity is important for the chaperone activity of BiP, BiP ATPase activity was not affected by KM04794 (Figure S6G). These results suggested that KM04794 at least controls the BiP activity with direct interaction.

Discussion

ER stress and UPR signaling are important for metabolic diseases. In particular, chronic ER stress and dysregulated UPR signaling are significant causes of the dysfunction and death of pancreatic β cells in type 2 diabetes (Fonseca et al., 2011; Rabhi et al., 2014). Therefore, improvement of ER function and intervention of the UPR in pancreatic β cells may be useful therapeutic strategies for type 2 diabetes. Several studies in human patients have provided potential treatments for type 2 diabetes and metabolic disease by these strategies. However, known chemicals may not adequately reduce ER stress and improve pancreatic β cell function. Chemical chaperone-like molecules and UPR regulators from diverse sources are needed to overcome the inadequacy of known chemicals to restore pancreatic β cells. Here, we identified a novel ER stress-reducing small molecule, KM04794, by utilizing a UPR-mediated transcriptional response system in a cell-based assay. KM04794 dramatically upregulated intracellular and secreted insulin in pancreatic β cells. KM04794 even restored the biosynthesis and secretion of a genetic insulin mutant. Our study has established chemical screening targeting the alleviation of ER stress as an attractive method for restoring pancreatic β cell function in metabolic diseases.

We report the discovery of a previously unrecognized small molecule, KM04794, which acts as chemical chaperone-like alleviator of ER stress. One advantage of KM04794 is its effectiveness against various causes of ER stress, similar to classical chemical chaperones. Since various proteins as well as insulin trigger ER stress even in pancreatic β cells in type 2 diabetes, efficacy against diverse stressors is an advantage for disease application. In addition, the effects of KM04794 were stronger (at the μM order) than those of 4PBA (at the mM order). Utilization of KM04794 at such a low dose could reduce side effects and toxicity. According to our results, KM04794 cannot efficiently inhibit ER stress caused by DTT. DTT directly affects UPR activation and chaperone functions, such as those of protein disulfide isomerase, as well as the accumulation of unfolded proteins (Eletto et al., 2014; Nadanaka et al., 2007; Oka et al., 2019). These functional changes by DTT may overcome the effects of KM04794 on ER stress and UPR signaling. Further characterization of KM04794 and comparison to other stressors and mutant proteins that cause ER stress are required before applying KM04794 to other diseases. Unfortunately, we could not detect KM04794 in plasma in C57BL/6J mice treated orally with KM04794, indicating its poor

bioavailability in mice. Our current focus is on the development of a derivative of KM04794 with enhanced bioactivity and bioavailability to allow *in vivo* testing.

Proteomic analysis of KM04794-binding proteins revealed their accumulation in the ER. In particular, the most abundant protein to bind KM04794 is BiP, an ATP-dependent HSP70-type chaperone that is most abundant in the ER (Behnke et al., 2015; Buck et al., 2007). The knockdown experiment showed that only BiP reduced the increase in insulin contents induced by KM04794. KM04794 led to a decreased interaction between BiP and insulin in cells. Our *in vitro* results showed that KM04794 could bind recombinant BiP and enhance its antiaggregation activity against denatured GAPDH protein, supporting the important role of BiP in the effects of KM04794. Members of the HSP70 chaperone family, including BiP, associate with, retain and dissociate from substrates in cooperation with a cochaperone (Pobre et al., 2019). The reduction in the interaction and ER stress suggest that this chaperone cycle may be accelerated by KM04794. The function of BiP is post-translationally regulated by its conformational change, oligomerization, modification and interaction with cochaperones (Behnke et al., 2015; Mapa et al., 2010; Marcinowski et al., 2011; Preissler et al., 2015b, 2015a; Wieteska et al., 2017). Conformational regulation of BiP by cochaperone SIL11 (Bap) is important for ER proteostasis in pancreatic β cells (Ittner et al., 2014; Rosam et al., 2018). Preissler et al. reported that the monomeric form of BiP, unlike the oligomeric form, efficiently inhibited the UPR (Preissler et al., 2015a). In addition, many other factors are involved in the interactions between BiP and its substrates, and these factors may differ depending on the substrate. Surprisingly, aggregation of insulin was increased by BiP alone and further enhanced by KM04794 (Figure S6G), and BiP ATPase activity was not affected solely by KM04794. Our results suggested that the effect of KM04794 might modulate the BiP chaperoning pathway. Therefore, we cannot the eliminate possibility that the 20 other candidate proteins might be involved in the KM04794-induced insulin induction and this issue needs to be further pursued. Although the direct mechanism has not been well elucidated, KM04794 may regulate the interaction between BiP and substrates to alleviate ER stress and induce insulin production.

In addition to the modulation of ER stress, KM04794 increased intracellular insulin by inhibiting insulin degradation but did not change insulin biosynthesis in pancreatic β cells. Because direct inhibition of degradation systems, including the proteasome and autophagy, impairs glucose-stimulated insulin

secretion, the effect of KM04794 must involve another mechanism (Ebato et al., 2008; Jung et al., 2008; Kitiphongspattana et al., 2005). We found that the effect of KM04794 on insulin was lost in MIN6m9 cells with partial BiP knockdown, suggesting the critical role of BiP in insulin induction by KM04794. A portion of newly synthesized insulin is misfolded and degraded through ER-associated degradation (ERAD) or autophagy, similar to the degradation of other proteins. Therefore, KM04794-induced enhancement of BiP activity may support insulin folding, leading to a decrease in insulin degradation and an increase in intracellular insulin levels. This hypothesis is supported by previous reports showing an increase in intracellular and secreted insulin due to BiP overexpression or precise BiP regulation by the cochaperone SIL1 (Ittner et al., 2014; Zhang et al., 2009). Furthermore, KM04794 showed antiaggregation activity against *Akita* mutant insulin, whose aggregation was prevented by BiP activity (Cunningham et al., 2019). These data also suggest that KM04794 enhances the effect of BiP on insulin biosynthesis. Unlike KM04794, the classical chemical chaperones 4PBA and TUDCA could not induce intracellular insulin production in our system. Restoration of insulin folding may be easily achieved through the enhancement of endogenous molecular chaperone function.

Insulin-positive β cells are reduced, and proper insulin biosynthesis is impaired in type 2 diabetes. While intervention to increase insulin biosynthesis in the remaining β cells may be an effective treatment, the hypersynthesis of proinsulin increases misfolding, leading to stress and β cell exhaustion (Arunagiri et al., 2018; Liu et al., 2005). Based on our study, a subset of ER proteostasis modulators could induce proper insulin biosynthesis as well as insulin secretion and cell survival in pancreatic β cells. The ER-targeted treatment may have new therapeutic strategy for dysfunction in pancreatic β cells in type 2 diabetes.

Significance

Endoplasmic reticulum (ER) stress and the unfolded protein response (UPR) are known to cause diabetes, especially resulting in pancreatic β cell dysfunction. Many studies identified small molecules that improve ER proteostasis or control UPR signaling. However, few compounds have been found to improve insulin synthesis and secretion through the regulation of ER proteostasis in pancreatic β cells. Here, we report the identification of a new small molecule, namely, KM04794, that alleviates ER stress by cell-based phenotypic screening of UPR signaling. KM04794 inhibited UPR signaling caused by ER stress induced by diverse chemicals. Protein aggregation and cell death were also alleviated by KM04794. Treatment of pancreatic β cells expressing mutant *Akita* insulin, which is known to induce ER stress as a proteotoxin, with KM04794 led to down-regulation of UPR target genes and insulin misfolding. In addition to exerting ameliorative effects on ER stress, KM04794 increased intracellular insulin in pancreatic β cells and primary islets. The chemoproteomic analysis using a photo-activated derivative of KM04794 revealed accumulation in the ER. Furthermore, the molecular chaperone BiP directly bound to KM04794 and may be a candidate target protein of KM04794 related to improvement in ER proteostasis. Our study not only reveals a new small molecule to improve ER proteostasis but also suggests that targeting ER proteostasis may improve aspects of pancreatic β cell dysfunction, especially insulin synthesis.

Acknowledgments

We thank Daiki Sato, Eisuke Kuraoka, Kazue Tsugawa and Miho Oyadomari for providing technical support and Chizuko Kimura for assistance with the manuscript preparation. We also thank David Ron for the kind gifts of the CHO:CHOP-GFP cell line and anti-XBP1 antibody and Jun-ichi Miyazaki and Susumu Seino for the kind gift of the MIN6m9 cell line. This work was supported by a Grant-in-Aid for Scientific Research (KAKENHI) from the Japan Society for the Promotion of Science (JSPS) (grant numbers JP20K08909 to M.M. and JP19H02853 to S.O.).

Author contributions

M.M. designed and performed most experiments. M.S. and K.K. performed the islet experiment. A.S., M.D. and A.O. synthesized the small-molecule probe. T.S. performed the *in vitro* aggregation experiment. N.S. generated the anti-ATF6α antibody. H.K. carried out the mass spectrometry analysis. S.O. planned the study and supervised the research. M.M. and S.O. interpreted the data. M.M. wrote the manuscript. All authors contributed to the discussion and reviewed/edited the manuscript.

Declarations of interest

No potential conflicts of interest relevant to this article are reported.

STAR Methods

Lead Contact and Material Availability

Further information and requests for resources and reagents should be directed to and will be fulfilled by the Lead Contact, Masato Miyake (miyake@genome.tokushima-u.ac.jp), or the co-corresponding author, Seiichi Oyadomari (oyadomar@genome.tokushima-u.ac.jp). All unique/stable reagents generated in this study are available from the Lead Contact with a completed Materials Transfer Agreement, with reasonable compensation for processing and shipping.

Experimental Model and Subject Details

Cell culture

C2C12 myoblasts and HEK293T and 3T3L1 cells were cultured in Dulbecco's modified Eagle's medium (DMEM) with 10% fetal bovine serum. Confluent 3T3L1 preadipocytes were induced to differentiate in medium containing 10% FBS, 10 μg/ml insulin, 1 μM rosiglitazone, 0.5 mM isobutylmethylxanthine (IBMX), and 0.4 μg/ml dexamethasone for 2 d and subsequently cultured in DMEM containing 10% FBS and 5 μg/ml insulin for an additional 6 d. The pancreatic β cell line MIN6m9, a kind gift from Jun-ichi Miyazaki (Osaka University) and Susumu Seino (Kobe University), was cultured in DMEM with 10% fetal bovine serum and 50 μM 2-mercaptoethanol (Minami et al., 2000). MEFs were cultured in DMEM with 10% fetal bovine serum, nonessential amino acids (Wako) and 50 μM 2-mercaptoethanol. CHO:CHOP-GFP cells, a kind gift from David Ron, were cultured in Ham's F-12 with 10% fetal bovine serum (Sekine et al., 2016). A pancreatic β cell line derived from *Akita* (InsC96Y/+) mice was established as previously described and cultured in DMEM with 10% fetal bovine serum and 50 μM 2-mercaptoethanol (Nozaki et al., 2004). All cell lines were confirmed to be mycoplasma-free. Reagent treatment conditions are indicated in the figure legends.

Animals

The Animal Research Committee of the University of Tokushima approved this study. Wild type C57/BL6J mice were purchased from Nippon SLC. The mice were maintained in a specific pathogen-

free environment (23 ± 2°C, 55 ± 5%) on a 12-h light/12-h dark cycle with food and water supplied *ad libitum*.

Method Details

Plasmid construction

Three tandem response elements, the ER stress-response element (ERSE: CCTTCACCAATCGGCGGCCTCCACGACGG), UPR element (UPRE: CTCGAGACAGGTGCTGACGTGGCATTC), and amino acid-response element (AARE: *AACATTGCATCATCCCCGC*), were used to replace the cAMP-response element of the pGL4.29 vector (Promega). Wild-type and *Akita* mutant insulin was cloned into a lentivirus vector based on pFUGW in which the CMV promoter replaced the TRE3G promoter derived from the Tet-On 3G Inducible Expression System (Clonetech). Mouse *BiP* was amplified by PCR and cloned into the pET16b vector (Millipore). For the CRISPR/Cas9 and CRISPR interference (CRISPRi) system, a DNA oligo targeting each gene was cloned into the lentiGuide-Puro vector (Addgene: 52963). The sequences of the DNA Oligos are obtained from Mouse Genome-wide CRISPRi-v2 Libraries (Horlbeck et al., 2016) and listed in table S2. The DNA sequence of each construct was verified with an ABI 3130 DNA sequencer (Thermo Fisher Scientific).

Generation of C2C12 and MIN6m9 reporter cell lines

Reporter cell lines were established as previously described (Miyake et al., 2016). In brief, C2C12 and MIN6m9 cells were transfected with a pGL4-based luciferase reporter vector using polyethylenimine MAX (Wako). Cells were selected with 200 μg/ml hygromycin, followed by limiting dilution cloning. The clone with the highest response to tunicamycin (Tm) was used in this study.

Generation of inducible *Akita* mutant insulin-expressing MIN6m9 and HEK293 cells

Lentiviruses were generated in HEK293T cells by cotransfection of the cells with the TRE3G-*Akita* mutant insulin transfer plasmid, the pMD2.G (Addgene: 12259) plasmid and the psPAX2 (Addgene: 12260) plasmid using polyethylenimine MAX (Wako). After 72 h of transfection, harvested lentiviruses

were centrifuged and filtered. MIN6m9 or HEK293 cells expressing Tet3G were transduced with lentivirus for TRE3G-wild type insulin or TRE3G-*Akita* mutant insulin expression and selected with 2 μg/ml puromycin.

Generation of knockout and knockdown MIN6m9 cells

Lentiviruses were generated with the lentiGuide-Puro-based vector, HR-SFFV-KRAB-dCas9-P2A-mCherry (Addgene: 60954) or lentiCas9-Blast (Addgene: 52962) and transduced as described above. Cells expressing the KRAB-dCas9 fusion protein were sorted using an S3 cell sorter (Bio-Rad). Cells expressing Cas9 were selected with 10 μg/ml blasticidin. Cells expressing sgRNA were selected with 2 μg/ml puromycin. Experiments were performed within 7 days after transduction of the sgRNA-expressing virus to avoid side effects from BiP downregulation.

Reporter assay

Luciferase reporter cells were seeded onto clear-bottom white 96-well plates (C2C12: 1×10^4 cells and MIN6m9: 3×10^4 cells) and treated with each chemical. For Tg and DTT treatment, cells were pretreated with KM04794 for 30 min. Luciferase activity was measured using the ONE-Glo Luciferase Assay System (Promega) according to the manufacturer's instructions. Luminescence was read on an EnVision plate reader (PerkinElmer). CHO:CHOP-GFP cells were seeded onto 6-well plates and treated with each chemical. Then, the cells were trypsinized and harvested. GFP fluorescence was measured using an S3 cell sorter (Bio-Rad).

Cell viability and survival assays

Reporter cells were seeded onto 96-well plates (C2C12: 1×10^4 cells and MIN6m9: 3×10^4 cells). After chemical treatment, cell viability was monitored using Cell Count Reagent SF (Nacalai Tesque) according to the manufacturer's instructions. The absorbance was measured using an EMax Plus microplate reader (Molecular Devices). The assay used to determine MEF survival was performed as reported previously (Lu et al., 2004). In brief, MEFs were plated at a density of 5×10^3 cells per 6-well plate and treated with Tm or Tm and KM04794 or 4PBA for 16 h. After the cells were washed with PBS,

they were allowed to recover and resume growth for 4 days. Colonies consisting of surviving cells were visualized with crystal violet (Wako) after fixation with 10% formalin. The data shown were obtained from representative wells from experiments repeated four times. Absorbance was measured after lysis with 2% SDS using an EMax Plus microplate reader (Molecular Devices).

RNA analysis

Total RNA was extracted from the cells according to the acid guanidinium thiocyanate-phenol-chloroform extraction method and used as templates for cDNA synthesis using ReverTra Ace qPCR RT Master Mix with gDNA Remover (Toyobo). The Prism 7900HT Real-Time PCR System (Life Technologies) or Step One Plus Real-Time PCR System (Life Technologies) and AmpliTaq Gold 360 Master Mix (Life Technologies) plus EvaGreen were used for qPCR analyses. The primer sequences are listed in Table S2. β-Actin (Actb) served as an internal control.

Generation of monoclonal antibody against ATF6α

This animal study was conducted in accordance with the Japanese Law for the Humane Treatment and Management of Animals (Law No. 105, October 1, 1973). Prior to the animal study initiation, the outline of the animal study protocol had been reviewed by the Institutional Animal Care and Use Committee of the Central Pharmaceutical Research Institute, JT Inc. A peptide corresponding to rat ATF6α amino acid sequence 196-209 (PALMPLAKQQSIIS) was synthesized by SCRUM, Inc., and chemically linked to the carrier protein OVA (Thermo Fisher Scientific). Five-week-old female ICR mice (Charles River Laboratories Japan) were immunized with the OVA-conjugated synthetic peptide. Cells isolated from the popliteal, inguinal and iliac lymph nodes were fused with a mouse myeloma cell line, PAI (JCRB). Supernatants of the growing hybridomas were screened by enzyme-linked immunosorbent assays (ELISAs) using the immunizing peptide. The selected antibody, clone ATZ-09, was purified by Protein G Sepharose (GE Healthcare) and used for immunoblot analysis. Confirmation data of the antibody by ELISAs and immunoblot analysis are shown in Figure S7. The isotype of ATZ-09 is IgG2a/κ.

Protein analysis

493 Total cell lysates were extracted with RIPA buffer (50 mM Tris-HCl (pH 7.4), 150 mM NaCl, 0.1% SDS,
494 1% NP-40, 0.5% sodium deoxycholate) containing protease inhibitor cocktail (BioTools) and
495 phosphatase inhibitor cocktail (BioTools). Protein concentration was measured using the BCA method,
496 and immunoblot analysis was performed as reported previously (Miyake et al., 2016). The proteins were
497 detected using anti-PERK, anti-eIF2α, anti-phospho-eIF2α, anti-IRE1, anti-ATF4, anti-insulin (Cell
498 Signaling Technology), anti-phospho-IRE1 (Abcam), anti-XBP1 (kindly gifted from D. Ron), anti-
499 ATF6α (ATZ-09; described above), anti-BiP (BD Biosciences), anti-KDEL, anti-α-Tubulin, and anti-β-
500 actin (MBL) antibodies. Bands were detected using Immobilon Western Chemiluminescent HRP
501 Substrate (Millipore), and images were acquired using the EZ-Capture II cooled CCD camera system
502 (ATTO Co.). High-molecular-weight (HMW) insulin was detected as previously described (Arunagiri et
503 al., 2019; Jang et al., 2019). In brief, the samples were lysed in RIPA buffer containing protease inhibitor
504 cocktail (BioTools) and prepared in Laemmli sample buffer without (non-reducing) or with (reducing)
505 100 mM DTT. After boiling for 5 min, samples were resolved by SDS-PAGE in 4–12% Bis-Tris
506 NuPAGE gels (Invitrogen) at 200 V for 30 min. Nonreducing gels were incubated in a solution containing
507 25 mM DTT for 10 min at room temperature prior to electrotransfer. Anti-proinsulin antibody (Novus)
508 was used for detection. For immunoprecipitation, cells were lysed in lysis buffer (50 mM Tris (pH 7.4),
509 150 mM NaCl, 1% Triton X-100, 1 mM EDTA, and 10% glycerol) containing a protease inhibitor
510 cocktail (BioTools). The lysates were incubated with an anti-Proinsulin antibody (Novus) in lysis buffer
511 overnight at 4°C and subsequently immunoprecipitated using COSMOGEL Ig-Accept Protein G
512 (Nacalai Tesque). The immunoprecipitates were washed four times with lysis buffer and boiled in SDS
513 sample buffer. The eluted samples were analyzed by immunoblotting.
514
515 **[35S] Metabolic labeling**
516 MIN6m9 cells plated on 6-well plates were metabolically labeled in DMEM-Cys/-Met (Invitrogen)
517 supplemented with 10% dialyzed fetal bovine serum, 50 μM 2-mercaptoethanol, and EasyTag EXPRESS
518 [35S] protein labeling mix (Perkin Elmer) for 30 min. Then, the cells were washed with PBS twice and
519 lysed with RIPA buffer with a protease inhibitor cocktail (BioTools). After separation by SDS-PAGE,

the gels were dried, exposed to phosphorimager plates (GE Healthcare), and imaged with a Typhoon imager (GE Healthcare). Band intensities were quantified by densitometry in ImageQuant.

BiP detection in a protein aggregate complex

Detection of BiP in protein aggregate complexes was performed as previously reported (Marciniak et al., 2004). In brief, after treatment with 1 μg/ml Tm and 20 μM KM04794 for 12 h, MEFs were incubated for 5 min with ice-cold PBS containing 20 mM N-ethylmaleimide and lysed in lysis buffer (0.5% Triton X-100, 20 mM HEPES (pH 7.5), 250 mM sucrose, 100 mM NaCl, 2.5 mM $CaCl_2$, and protease inhibitor cocktail). Post-nuclear supernatant was prepared from the lysate by centrifugation at 15,000 ×g for 15 min at 4°C. The total protein (1 mg) amount was adjusted with 0.8% SDS, and the total protein was then layered on a cushion of 20% glycerol, 20 mM HEPES (pH 7.5), 0.5% Triton X-100, and 0.8% SDS. Samples were centrifuged at 100,000 ×g for 45 min at 4°C. The resulting pellet was resuspended in urea loading buffer (9.6 M urea, 12% glycerol, 1.36% SDS, 40 mM Tris (pH 6.8), 0.002% bromophenol blue, with or without 100 mM DTT as indicated), heated to 95°C for 5 min, and separated by SDS-PAGE for immunoblotting.

Glucose stimulated-insulin secretion (GSIS) analysis

MIN6m9 cells were plated on 96-well plates (4×10^4 cells), cultured overnight and treated with reagents as described in the figure legend. After washing with PBS twice, the cells were preincubated in Krebs-Ringer bicarbonate HEPES (KRBH) buffer (10 mM HEPES, 119 mM NaCl, 4.74 mM KCl, 1.19 mM $MgCl_2$ $6H_2O$, 1.19 mM KH_2PO_4, 2.54 mM $CaCl_2$, 25 mM $NaHCO_3$, 0.5% BSA) containing 1.4 mM glucose for 30 min and cultured with KRBH buffer containing 2.8, 16.7 or 25 mM glucose for 1 h. The insulin levels in the medium and cells lysed with acid-EtOH were analyzed using the AlphaLISA human insulin immunoassay kit (Perkin Elmer), Insulin High Range Assay kit HTRF (CisBio), LBIS Mouse Insulin ELISA kit (S-type: WAKO) or Rat/Mouse Proinsulin ELISA (Mercodia) according to the manufacturer's instructions.

Pancreatic islet isolation and GSIS analysis

548 Pancreatic islets were prepared from the wild-type C57/BL6J mouse pancreas. HBSS (0.8% NaCl, 5.36
549 mM KCl, 0.34 mM Na_2HPO_4, 0.44 mM KH_2PO_4, 0.1% glucose, 1.26 mM $CaCl_2$, 0.4 mM $MgSO_4$, 0.49
550 mM $MgCl_2$, and 4.2 mM $NaHCO_3$) was used for perfusion and washing of the pancreas. Collagenase
551 type IV (Worthington Biochemical) was dissolved in ice-cold HBSS to a final concentration of 2.5 mg/ml.
552 The pancreas was perfused from the common bile duct using 2.5 ml of the collagenase solution and
553 incubated at 37°C for 25 min. The collagenase was disabled with RPMI 1640 medium (containing 10%
554 fetal bovine serum, sodium pyruvate, 1 mM HEPES, 50 μM β-mercaptoethanol and 1% penicillin-
555 streptomycin), after which the collagenase-treated pancreas was crushed by pipetting using a 10-ml
556 pipette tube (Thermo Fisher). Islets were selected using a dissecting microscope and placed into Petri
557 dishes. Five size-matched islets were collected in a single PCR tube, treated with KM04794 for 8 h, and
558 preincubated with KRBH buffer containing 2.8 mM glucose for 30 min. Islets were grown for 45 min
559 under 100 μL of 2.8 mM glucose/KRBH, after which the medium was collected, and the islets were then
560 grown under 100 μL of 25 mM glucose/KRBH for 45 min. Insulin secreted into the KRBH was measured
561 with an Insulin High Range Assay kit HTRF (CisBio). The amount of secreted and intracellular insulin
562 was normalized to the amount of total cellular protein.
563
564 **Treatment with CM**
565 MIN6m9 cells were plated in 6-well plates (1.2×10^6 cells) and treated with DMSO, 20 μM KM04794, 1
566 μg/ml Tm or 1 μg/ml Tm and 20 μM KM04794 for 8 h; GSIS analysis was performed in KRBH buffer
567 containing 16.7 mM glucose as described above. After GSIS analysis, the KRBH buffer was centrifuged
568 for 5 min at 3,000 ×g. The supernatants were collected as CM and stored at -80°C until use. KRBH buffer
569 containing 16.7 mM glucose was used as a negative control. Insulin (10 nM) was used as a positive
570 control. Differentiated 3T3L1 adipocytes were precultured with FBS-free DMEM for 6 h, washed with
571 PBS twice and treated with prewarmed CM for 15 min. After washing with PBS, the cells were lysed as
572 described above and analyzed by immunoblotting using an anti-P-Akt or anti-Akt antibody (Cell
573 Signaling Technology).
574
575 **Pulldown assay with KM04794-probe in cell lysates and recombinant protein**

MIN6m9 cells and MEFs were treated with 1 μg/ml Tm and 20 μM KM04794-probe in the presence or absence of 100 μM KM04794 (competitor) for 3 h at 37°C. Photoirradiation was performed on ice for 10 min using the UVL-56 ultraviolet lamp (365 nm, 6 W, from a distance of 1 cm: UVP). The cells were lysed with 20 mM HEPES, 150 mM NaCl and 1% NP-40 on ice. Purified BiP (0.4 μM) mixed with the indicated amount of KM04794-probe was incubated for 30 min at 25°C. Cell lysate samples or total purified protein sample mixtures containing 400 μg of protein were reacted with 5 mM tris(3-hydroxypropyltriazolylmethyl)amine (THPTA), 1 mM copper(II) sulfate ($CuSO_4$), 15 mM sodium ascorbate and 250 μM biotin-$dPEG_{11}$-azide (Quantabio) for 2 h at room temperature. The samples of purified BiP were subjected to immunoblot analysis using streptavidin-HRP (Thermo Fisher). The samples from live cells were then precipitated from the reaction mixture by the addition of an equal volume of 3:1 chloroform/methanol. The pellet was washed twice with methanol. The precipitate was suspended in 4% SDS, 20 mM EDTA and 10% glycerol in PBS. Suspended samples were diluted 10-fold with PBS and mixed with high-performance streptavidin-Sepharose (GE Healthcare). This suspension was placed on a rotator and incubated for 2 h at room temperature. The beads were centrifuged and washed twice with RIPA buffer and three times with PBS containing 1% SDS. Mass spectrometry was performed as described below to identify proteins. For immunoblot analysis, proteins were eluted with elution buffer (62.5 mM Tris-HCl (pH 6.8), 2% SDS, 12.5% glycerol and 4 mM biotin) and subjected to immunoblot analysis using an anti-KDEL antibody (MBL).

Mass spectrometry

After pulldown, the beads from two biological replicates per sample were further washed twice with ammonium bicarbonate. Proteins on the beads were digested by the addition of 200 ng of trypsin (MS grade, Pierce) at 37°C for 16 h. The digested products were reduced, alkylated, acidified, and desalted using GL-Tip SDB (GL Sciences). The eluates were evaporated in a SpeedVac concentrator and dissolved in 0.1% trifluoroacetic acid and 3% acetonitrile (ACN). LC-MS/MS analysis of the resultant peptides was performed on an EASY-nLC 1200 UHPLC connected to a Q Exactive Plus mass spectrometer through a nanoelectrospray ion source (Thermo Fisher Scientific). The peptides were separated on a 75-μm inner diameter × 150 mm C18 reversed-phase column (Nikkyo Technos) with a

linear 4–32% ACN gradient for 0–100 min followed by an increase to 80% ACN for 10 min. The mass spectrometer was operated in data-dependent acquisition mode with the top 10 MS/MS method. MS1 spectra were measured at a resolution of 70,000 with an automatic gain control (AGC) target of 1×10^6 and a mass range from 350 to 1,500 *m/z*. HCD MS/MS spectra were triggered at a resolution of 17,500, an AGC target of 5×10^4, an isolation window of 2.0 *m/z*, a maximum injection time of 60 msec, and a normalized collision energy of 27. Dynamic exclusion was set to 10 sec. Raw data were directly analyzed against the SwissProt database restricted to *Mus musculus* using Proteome Discoverer version 2.2 (Thermo Fisher Scientific) with Mascot search engine version 2.5 (Matrix Science). The search parameters were as follows: (a) trypsin as the enzyme with up to two missed cleavages, (b) a precursor mass tolerance of 10 ppm, (c) a fragment mass tolerance of 0.02 Da, (d) carbamidomethylation of cysteine as a fixed modification, and (e) acetylation of the protein N-terminus and oxidation of methionine as variable modifications. Peptides were filtered at a false discovery rate of 1% using the percolator node. Label-free precursor ion quantification was performed using precursor ion quantifier node, and normalization was performed such that the total sum of abundance values for each sample over all peptides was the same. Proteins that were peptide spectrum matches (PSMs) > 10 and peptides > 2 were adopted for subsequent analysis. GO enrichment was performed with g:Profiler (https://biit.cs.ut.ee/gprofiler/gost).

Protein purification

Mouse BiP encoded in the pET16b plasmid was expressed in BL21 (DE3) *E. coli* cells (Millipore) as described previously (Preissler et al., 2015a). In brief, bacterial cultures were grown at 37°C in LB medium containing 100 µg/ml ampicillin to an optical density (OD600 nm) of 0.6, and expression was induced with 50 µM isopropyl β-D-1-thiogalactopyranoside (IPTG). After incubation for 8 h at 30°C, the cells were centrifuged, and the pellets were sonicated in lysis buffer (50 mM Tris–HCl (pH 7.5), 500 mM NaCl, 1 mM $MgCl_2$, 0.2% Triton X-100, 10% glycerol, 20 mM imidazole and protease inhibitor cocktail (BioTools)). The lysates were cleared by centrifugation for 30 min at 20,000 ×g and incubated with 500 µl of COSMOGEL His-Accept (Nacalai Tesque) per 1 L of expression culture for 2 h at 4°C. The beads were washed five times with 20 bed volumes of lysis buffer sequentially supplemented with

30 mM imidazole, 1% Triton X-100, 1 M NaCl, or 0.5 M Tris–HCl (pH 7.5). Bound BiP protein was eluted in 50 mM Tris–HCl (pH 7.5), 500 mM NaCl, 1 mM $MgCl_2$, 10% glycerol, and 250 mM imidazole and dialyzed against HKM buffer (50 mM HEPES-KOH (pH 7.4), 150 mM KCl, 10 mM $MgCl_2$). The purified BiP protein was snap-frozen in liquid nitrogen and stored at -80°C.

GAPDH and insulin aggregation assay

The aggregation of denatured GAPDH from rabbit muscle (Sigma) was measured as described previously with some modifications (Kramer et al., 2004; Saio et al., 2014, 2018). GAPDH (125 μM) was denatured by 3 M guanidine-HCl in KMH buffer (50 mM HEPES-KOH (pH 7.5), 150 mM KCl, 10 mM $MgCl_2$) for 12 h at 4°C. The denatured enzyme was diluted 50-fold into KMH buffer containing 3 mM ATP with either 1 μM BiP, 10 μM KM04794 or both. Then, aggregation was monitored by 90° light scattering at 620 nm on a spectrofluorometer (FP-8500, JASCO Corporation). The experiment was carried out at 20°C. The aggregation of recombinant human insulin (50 μM: Wako) was induced by 1 mM DTT in KMH buffer in the presence or absence of BiP and KM04794 for 40 min at 37°C. Then, aggregation was monitored using a PROTEOSTAT Protein Aggregation Assay (Enzo Life Sciences) and an EnVision2102 system (Ex 480 nm, Em 595 nm, PerkinElmer) according to the manufacturer's instructions.

ATPase assay

BiP ATPase activity was measured using the Fluorospark Kinase/ADP Multi-assay Kit (WAKO) according to the manufacturer's instructions. Purified BiP samples (0.5 μM) and the indicated amount of KM04794 were incubated in HKM with 30 μM ATP for 60 min at 30°C. Each sample was then mixed with 2× detection reagent and incubated for 30 min at 25°C. Fluorescence was measured with an EnVision plate reader (excitation: 540 nm, emission: 590 nm; PerkinElmer).

Statistical analyses

All results are expressed as the mean ± standard deviation (SD). The unpaired two-tailed Student's t-test was performed to determine p values for comparisons of paired samples. One-way ANOVA followed by

the Holm-Sidak multiple comparisons test was performed to determine p values for comparisons of more than three groups. All statistical analyses were performed using Excel (Microsoft) or R (R Project) software. Differences with a p value < 0.05 were considered statistically significant.

Chemical synthesis

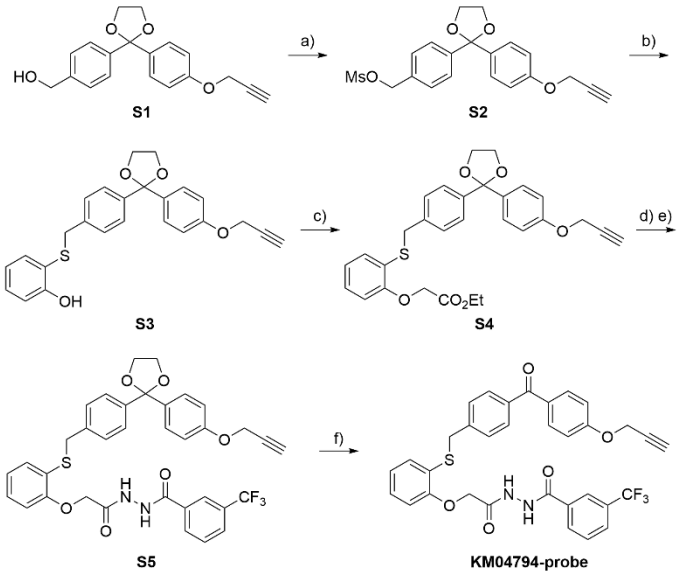

Scheme: Reagents and conditions: a) methanesulfonyl chloride (MsCl), Et_3N, $Me_3N \cdot HCl$, toluene, 78%; b) 2-mercaptophenol, K_2CO_3, DMF, quant.; c) ethyl bromoacetate, K_2CO_3, acetone, reflux, 97%; d) $LiOH \cdot H_2O$, THF, H_2O; e) 3-(trifluoromethyl)benzohydrazide, *N*,*N*-carbonyldiimidazole (CDI), dichloromethane (DCM), 60% (2 steps); f) HCl aq., THF, 78%.

General methods

All reactions were carried out under a positive pressure of argon at room temperature unless otherwise noted. For column chromatography, silica Gel 60 N (spherical, neutral, Kanto Chemical Co. Inc.) was employed. NMR spectra were recorded using a Bruker AV400N at 400 MHz frequency for ^1H and 100 MHz frequency for ^{13}C and a Brucker AV500 at 125 MHz frequency for ^{13}C. ^1H and ^{13}C NMR chemical sifts are reported in parts per million and are calibrated to the residual solvent signal ($CHCl_3$: ^1H NMR: δ [ppm] = 7.26, ^{13}C NMR: δ [ppm] = 77.16). The multiplicity of the signals is given

as follows: s: singlet, d: doublet, t: triplet, q: quartet, br: broad, m, multiplet). Coupling constants, *J*, are reported in Hertz [Hz]. Mass spectra were recorded on a Waters Micromass® LCT PremierTM (ESI-TOF).

Mesylate S2

To a solution of alcohol **S1** (200 mg, 0.46 mmol) (Yarravarapu et al., 2018), Et_3N (446 μL, 3.2 mmol), and $Me_3N{\cdot}HCl$ (6.1 mg, 0.064 mmol) (Yoshida et al., 1999) in toluene (6.4 mL) was added MsCl (74.2 μL, 0.96 mmol) at 0 °C, and the obtained solution was stirred at room temperature for 1.5 h. After quenching by the addition of water, the mixture was extracted with EtOAc. After the sample was washed with water and subsequent brine, the combined organic layer was dried over Na_2SO_4, filtered and concentrated in vacuo. The obtained **S2** (195 mg, 78%, white solid) was used in the subsequent experiment without further purification. ^{1}H NMR ($CDCl_3$, 400 MHz): δ = 2.51 (1H, brs), 2.91 (3H, s), 4.00-4.09 (4H, m), 4.66 (2H, d, J = 1.8 Hz), 5.21 (2H, s), 6.92 (2H, d, J = 8.7 Hz), 7.38 (2H, d, J = 7.7 Hz), 7.41 (2H, d, J = 8.7 Hz), 7.55 (2H, d, J = 7.7 Hz); ^{13}C NMR ($CDCl_3$, 100 MHz): δ = 38.3, 55.8, 64.9, 71.0, 75.7, 78.4, 109.0, 114.5, 126.8, 127.5, 128.7, 133.1, 134.9, 143.6, 157.5; HRMS (ESI-TOF) *m/z*: $[M+Na]^+$ Calcd for $C_{20}H_{20}NaO_6S$ 411.0878; found 411.0863.

Phenol S3

K_2CO_3 (256 mg, 1.85 mmol) and 2-mercaptopheol (191 μL, 1.85 mmol) were added to mesylate **S2** (145 mg, 0.37 mmol) in DMF (3.7 mL), and the mixture was stirred for 21.5 h. Then, water was added to the reaction mixture. After extraction with EtOAc, the combined organic layer was successively washed with 1 M NaOH aq., water, and brine. After drying over Na_2SO_4, the extract was filtered and concentrated in vacuo. The obtained **S3** (colorless oil, 162 mg, quant.) was used in the next reaction without further purification. ^{1}H NMR ($CDCl_3$, 400 MHz) δ = 2.51 (1H, t, J = 2.4 Hz), 3.84 (2H, s), 3.98-4.09 (4H, m), 4.67 (2H, d, J = 2.4 Hz), 6.52 (1H, s), 6.77 (1H, td, J = 7.5 and 1.2 Hz), 6.90-6.94 (3H, m), 7.06 (2H, d, J = 8.3 Hz), 7.21-7.26 (2H, m), 7.38 (4H, m); ^{13}C NMR ($CDCl_3$, 125 MHz): δ = 41.0, 55.8, 64.9, 75.6, 78.5, 109.2, 114.4, 114.8, 118.2, 120.6, 126.6, 127.7, 128.6, 131.4, 135.1, 136.4,

137.3, 141.3, 157.1, 157.5; HRMS (ESI-TOF) *m/z*: $[M+Na]^+$ Calcd for $C_{25}H_{22}NaO_4S$ 441.1137; Found 411.1146.

Ether S4

To a solution of phenol **S3** (53.3 mg, 0.13 mmol) and ethyl bromoacetate (14.3 μL, 0.13 mmol) in acetone (2.6 mL) was added K_2CO_3, and the resulting suspension was refluxed for 9.5 h. After filtration of the reaction mixture, the obtained filtrate was concentrated in vacuo to give **S4** (63.3 mg, 97%) as a colorless oil. ^{1}H NMR ($CDCl_3$, 400 MHz) δ = 1.29 (3H, t, J = 7.1 Hz), 2.51 (1H, t, J = 2.5 Hz), 3.98-4.07 (4H, m), 4.14 (2H, s), 4.27 (2H, q, J = 7.2 Hz), 4.67 (2H, d, J = 2.5 Hz), 4.67 (2H, s), 6.73 (1H, d, J = 8.2 Hz), 6.88 (1H, td, J = 7.6 and 1.1 Hz), 6.91 (2H, d, J = 9.0 Hz), 7.16 (1H, td, J = 8.2 and 1.6 Hz), 7.23-7.28 (3H, m), 7.38 (2H, d, J = 9.0 Hz), 7.39 (2H, d, J = 8.3 Hz); ^{13}C NMR ($CDCl_3$, 125 MHz): δ = 14.2, 37.1, 55.8, 61.4, 64.8, 65.9, 75.6, 78.5, 109.3, 111.9, 114.4, 122.1, 125.0, 126.3, 127.7, 127.9, 128.8, 131.7, 135.2, 137.5, 140.9, 156.3, 157.4, 168.6; HRMS (ESI-TOF) *m/z*: $[M+Na]^+$ Calcd for $C_{29}H_{28}NaO_6S$ 527.1504; found 527.1486.

Hydrazide S5

$LiOH \cdot H_2O$ (49.0 mg, 1.19 mmol) was added to a solution of ester **S4** (300 mg, 0.59 mmol) in THF/H_2O (1/1 (v/v), 4.0 mL), and the resulting mixture was stirred for 75 min. After concentration in vacuo, DCM (2.0 mL) and CDI (101 mg, 0.62 mmol) were added to the residue. After 1 h of stirring, 3-(trifluoromethyl)benzohydrazide (127 mg, 0.62 mmol) was added. After being stirred for 13 h, the reaction was quenched by addition of water. The obtained mixture was extracted with EtOAc, and the combined organic layer was washed with water (2 times) and brine, dried over Na_2SO_4, filtered, and concentrated in vacuo. The obtained residue was purified by column chromatography (hexane/EtOAc = 2/1 to 3/2 [v/v]), and hydrazide **S5** (177.1 mg, 60%) was obtained as a colorless oil. ^{1}H NMR ($CDCl_3$, 400 MHz) δ = 2.50 (1H, t, J = 2.4 Hz), 3.96-4.07 (4H, m), 4.01 (2H, s), 4.54 (2H, s), 4.66 (2H, d, J = 2.4 Hz), 6.82 (1H, d, J = 8.0 Hz), 6.90 (2H, d, J = 8.8 Hz), 7.02 (1H, td, J = 7.7 and 0.9 Hz), 7.13 (2H, d, J = 8.2 Hz), 7.28 (1H, td, J = 8.0 and 1.5 Hz), 7.33 (2H, d, J = 8.2 Hz), 7.34 (2H, d, J = 8.8 Hz), 7.45 (1H, dd, J = 7.7 and 1.5 Hz), 7.63 (1H, t, J = 7.8 Hz), 7.83 (1H, d, J = 7.8 Hz), 8.07 (1H, d, J = 7.8 Hz),

8.17 (1H, s), 8.87 (1H, d, J = 4.0 Hz), 8.95 (1H, d, J = 4.0 Hz); ^{13}C NMR ($CDCl_3$, 125 MHz): δ = 38.9, 55.8, 64.9, 67.6, 75.6, 78.5, 109.3, 112.7, 114.4, 122.5, 123.0, 124.6, 124.9, 126.3, 127.5, 128.5, 128.9, 129.3, 130.7, 131.0, 131.3, 132.3, 133.2, 135.0, 138.0, 141.0, 156.2, 157.5, 163.6, 166.0; HRMS (ESI-TOF) *m/z*: $[M+Na]^+$ Calcd for $C_{35}H_{29}F_3N_2NaO_6S$ 685.1596; found 685.1602.

Photoaffinity probe KM04794-probe

To a solution of acetal **S5** (46.3 mg, 0.070 mmol) in THF (1.4 mL) was added hydrochloric acid (6 M, 1.4 mL), and the mixture was stirred for 1 h. The reaction was quenched by addition of 1 M NaOH aq., and the mixture was extraction with EtOAc. The combined organic layer was washed with brine, dried over Na_2SO_4, filtered and concentrated in vacuo to give **KM04794-probe** (33.9 mg, 78%) as a white amorphous substance. ^{1}H NMR ($CDCl_3$, 400 MHz) δ = 2.56 (1H, t, J = 2.4 Hz), 4.14 (2H, s), 4.62 (2H, s), 4.77 (2H, d, J = 2.4 Hz), 6.86 (2H, d, J = 7.8 Hz), 6.99-7.04 (1H, m), 7.02 (2H, d, J = 8.9 Hz), 7.27-7.32 (1H, m), 7.31 (2H, d, J = 8.1 Hz), 7.40 (1H, dd, J = 7.7 and 1.4 Hz), 7.61-7.65 (1H, m), 7.63 (2H, d, J = 8.1 Hz), 7.78-7.84 (1H, m), 7.80 (2H, d, J = 8.9 Hz), 8.12 (1H, d, J = 7.7 Hz), 8.23 (1H, s), 9.08 (1H, br s), 9.20 (1H, d, J = 4.4 Hz); ^{13}C NMR ($CDCl_3$, 100 MHz): δ = 38.7, 55.9, 67.7, 76.2, 77.7, 112.8, 114.4, 123.1, 124.1, 124.7, 124.9, 128.6, 128.9, 129.2, 129.3, 129.9, 130.7, 131.0, 131.3, 132.0, 132.5, 133.4, 136.9, 142.4, 156.2, 161.1, 163.5, 165.7, 195.3; HRMS (ESI-TOF) *m/z*: $[M+Na]^+$ Calcd for $C_{33}H_{25}F_3N_2NaO_5S$ 641.1334; found 641.1328.

References

Arunagiri, A., Haataja, L., Cunningham, C.N., Shrestha, N., Tsai, B., Qi, L., Liu, M., and Arvan, P. (2018). Misfolded proinsulin in the endoplasmic reticulum during development of beta cell failure in diabetes. Ann. N. Y. Acad. Sci. *1418*, 5–19.

Arunagiri, A., Haataja, L., Pottekat, A., Pamenan, F., Kim, S., Zeltser, L.M., Paton, A.W., Paton, J.C., Tsai, B., Itkin-Ansari, P., et al. (2019). Proinsulin misfolding is an early event in the progression to type 2 diabetes. Elife *8*.

Back, S.H., and Kaufman, R.J. (2012). Endoplasmic reticulum stress and type 2 diabetes. Annu. Rev. Biochem. *81*, 767–793.

Behnke, J., Feige, M.J., and Hendershot, L.M. (2015). BiP and its nucleotide exchange factors Grp170 and Sil1: mechanisms of action and biological functions. J. Mol. Biol. *427*, 1589–1608.

Bruhat, A., Jousse, C., Carraro, V., Reimold, A.M., Ferrara, M., and Fafournoux, P. (2000). Amino acids control mammalian gene transcription: activating transcription factor 2 is essential for the amino acid responsiveness of the CHOP promoter. Mol. Cell. Biol. *20*, 7192–7204.

Buck, T.M., Wright, C.M., and Brodsky, J.L. (2007). The activities and function of molecular chaperones in the endoplasmic reticulum. Semin. Cell Dev. Biol. *18*, 751–761.

Clarke, H.J., Chambers, J.E., Liniker, E., and Marciniak, S.J. (2014). Endoplasmic reticulum stress in malignancy. Cancer Cell *25*, 563–573.

Cunningham, C.N., Williams, J.M., Knupp, J., Arunagiri, A., Arvan, P., and Tsai, B. (2019). Cells Deploy a Two-Pronged Strategy to Rectify Misfolded Proinsulin Aggregates. Mol. Cell *75*, 442-456.e4.

Duan, H., Li, Y., Arora, D., Xu, D., Lim, H.-Y., and Wang, W. (2017). Discovery of a benzamide derivative that protects pancreatic β-cells against endoplasmic reticulum stress. J. Med. Chem. *60*, 6191–6204.

775 Ebato, C., Uchida, T., Arakawa, M., Komatsu, M., Ueno, T., Komiya, K., Azuma, K., Hirose, T., Tanaka,
776 K., Kominami, E., et al. (2008). Autophagy is important in islet homeostasis and compensatory increase
777 of beta cell mass in response to high-fat diet. Cell Metab. *8*, 325–332.

778 Eizirik, D.L., and Cnop, M. (2010). ER stress in pancreatic beta cells: the thin red line between adaptation
779 and failure. Sci. Signal. *3*, e7.

780 Eletto, D., Eletto, D., Dersh, D., Gidalevitz, T., and Argon, Y. (2014). Protein disulfide isomerase A6
781 controls the decay of IRE1α signaling via disulfide-dependent association. Mol. Cell *53*, 562–576.

782 Fonseca, S.G., Gromada, J., and Urano, F. (2011). Endoplasmic reticulum stress and pancreatic β-cell
783 death. Trends Endocrinol. Metab. *22*, 266–274.

784 Fu, S., Yalcin, A., Lee, G.Y., Li, P., Fan, J., Arruda, A.P., Pers, B.M., Yilmaz, M., Eguchi, K., and
785 Hotamisligil, G.S. (2015). Phenotypic assays identify azoramide as a small-molecule modulator of the
786 unfolded protein response with antidiabetic activity. Sci. Transl. Med. *7*, 292ra98.

787 Ghiasi, S.M., Dahlby, T., Hede Andersen, C., Haataja, L., Petersen, S., Omar-Hmeadi, M., Yang, M.,
788 Pihl, C., Bresson, S.E., Khilji, M.S., et al. (2019). Endoplasmic Reticulum Chaperone Glucose-Regulated
789 Protein 94 Is Essential for Proinsulin Handling. Diabetes *68*, 747–760.

790 Ghosh, R., Wang, L., Wang, E.S., Perera, B.G.K., Igbaria, A., Morita, S., Prado, K., Thamsen, M.,
791 Caswell, D., Macias, H., et al. (2014). Allosteric inhibition of the IRE1α RNase preserves cell viability
792 and function during endoplasmic reticulum stress. Cell *158*, 534–548.

793 Grandjean, J.M.D., and Wiseman, R.L. (2020). Small molecule strategies to harness the unfolded protein
794 response: where do we go from here? J. Biol. Chem. *295*, 15692–15711.

795 Han, J., and Kaufman, R.J. (2017). Physiological/pathological ramifications of transcription factors in
796 the unfolded protein response. Genes Dev. *31*, 1417–1438.

797 Han, J., Song, B., Kim, J., Kodali, V.K., Pottekat, A., Wang, M., Hassler, J., Wang, S., Pennathur, S.,
798 Back, S.H., et al. (2015). Antioxidants complement the requirement for protein chaperone function to
799 maintain β-cell function and glucose homeostasis. Diabetes *64*, 2892–2904.

800 Harding, H.P., Zeng, H., Zhang, Y., Jungries, R., Chung, P., Plesken, H., Sabatini, D.D., and Ron, D.
801 (2001). Diabetes mellitus and exocrine pancreatic dysfunction in perk-/- mice reveals a role for
802 translational control in secretory cell survival. Mol. Cell *7*, 1153–1163.

803 Hartley, T., Siva, M., Lai, E., Teodoro, T., Zhang, L., and Volchuk, A. (2010). Endoplasmic reticulum
804 stress response in an INS-1 pancreatic beta-cell line with inducible expression of a folding-deficient
805 proinsulin. BMC Cell Biol. *11*, 59.

806 Hassler, J.R., Scheuner, D.L., Wang, S., Han, J., Kodali, V.K., Li, P., Nguyen, J., George, J.S., Davis,
807 C., Wu, S.P., et al. (2015). The IRE1α/XBP1s pathway is essential for the glucose response and
808 protection of β cells. PLoS Biol. *13*, e1002277.

809 Horlbeck, M.A., Gilbert, L.A., Villalta, J.E., Adamson, B., Pak, R.A., Chen, Y., Fields, A.P., Park, C.Y.,
810 Corn, J.E., Kampmann, M., et al. (2016). Compact and highly active next-generation libraries for
811 CRISPR-mediated gene repression and activation. Elife *5*.

812 Hotamisligil, G.S. (2010). Endoplasmic reticulum stress and the inflammatory basis of metabolic disease.
813 Cell *140*, 900–917.

814 Ittner, A.A., Bertz, J., Chan, T.Y.B., van Eersel, J., Polly, P., and Ittner, L.M. (2014). The nucleotide
815 exchange factor SIL1 is required for glucose-stimulated insulin secretion from mouse pancreatic beta
816 cells in vivo. Diabetologia *57*, 1410–1419.

817 Jang, I., Pottekat, A., Poothong, J., Yong, J., Lagunas-Acosta, J., Charbono, A., Chen, Z., Scheuner, D.L.,
818 Liu, M., Itkin-Ansari, P., et al. (2019). PDIA1/P4HB is required for efficient proinsulin maturation and
819 ß cell health in response to diet induced obesity. Elife *8*.

820 Jung, H.S., Chung, K.W., Won Kim, J., Kim, J., Komatsu, M., Tanaka, K., Nguyen, Y.H., Kang, T.M.,
821 Yoon, K.-H., Kim, J.-W., et al. (2008). Loss of autophagy diminishes pancreatic beta cell mass and
822 function with resultant hyperglycemia. Cell Metab. *8*, 318–324.

823 Kitakaze, K., Taniuchi, S., Kawano, E., Hamada, Y., Miyake, M., Oyadomari, M., Kojima, H., Kosako,
824 H., Kuribara, T., Yoshida, S., et al. (2019). Cell-based HTS identifies a chemical chaperone for
825 preventing ER protein aggregation and proteotoxicity. Elife *8*.

826 Kitiphongspattana, K., Mathews, C.E., Leiter, E.H., and Gaskins, H.R. (2005). Proteasome inhibition
827 alters glucose-stimulated (pro)insulin secretion and turnover in pancreatic {beta}-cells. J. Biol. Chem.
828 *280*, 15727–15734.

829 Kozuka, C., Sunagawa, S., Ueda, R., Higa, M., Tanaka, H., Shimizu-Okabe, C., Ishiuchi, S., Takayama,
830 C., Matsushita, M., Tsutsui, M., et al. (2015). γ-Oryzanol protects pancreatic β-cells against endoplasmic
831 reticulum stress in male mice. Endocrinology *156*, 1242–1250.

832 Kramer, G., Rutkowska, A., Wegrzyn, R.D., Patzelt, H., Kurz, T.A., Merz, F., Rauch, T.,
833 Vorderwülbecke, S., Deuerling, E., and Bukau, B. (2004). Functional dissection of Escherichia coli
834 trigger factor: unraveling the function of individual domains. J. Bacteriol. *186*, 3777–3784.

835 Lee, A.-H., Heidtman, K., Hotamisligil, G.S., and Glimcher, L.H. (2011). Dual and opposing roles of the
836 unfolded protein response regulated by IRE1alpha and XBP1 in proinsulin processing and insulin
837 secretion. Proc. Natl. Acad. Sci. U. S. A. *108*, 8885–8890.

838 Liu, M., Li, Y., Cavener, D., and Arvan, P. (2005). Proinsulin disulfide maturation and misfolding in the
839 endoplasmic reticulum. J. Biol. Chem. *280*, 13209–13212.

840 Lu, P.D., Jousse, C., Marciniak, S.J., Zhang, Y., Novoa, I., Scheuner, D., Kaufman, R.J., Ron, D., and
841 Harding, H.P. (2004). Cytoprotection by pre-emptive conditional phosphorylation of translation
842 initiation factor 2. EMBO J. *23*, 169–179.

Mapa, K., Sikor, M., Kudryavtsev, V., Waegemann, K., Kalinin, S., Seidel, C.A.M., Neupert, W., Lamb, D.C., and Mokranjac, D. (2010). The conformational dynamics of the mitochondrial Hsp70 chaperone. Mol. Cell *38*, 89–100.

Marciniak, S.J., Yun, C.Y., Oyadomari, S., Novoa, I., Zhang, Y., Jungreis, R., Nagata, K., Harding, H.P., and Ron, D. (2004). CHOP induces death by promoting protein synthesis and oxidation in the stressed endoplasmic reticulum. Genes Dev. *18*, 3066–3077.

Marcinowski, M., Höller, M., Feige, M.J., Baerend, D., Lamb, D.C., and Buchner, J. (2011). Substrate discrimination of the chaperone BiP by autonomous and cochaperone-regulated conformational transitions. Nat. Struct. Mol. Biol. *18*, 150–158.

Martínez, G., Khatiwada, S., Costa-Mattioli, M., and Hetz, C. (2018). ER Proteostasis Control of Neuronal Physiology and Synaptic Function. Trends Neurosci. *41*, 610–624.

Minami, K., Yano, H., Miki, T., Nagashima, K., Wang, C.Z., Tanaka, H., Miyazaki, J.I., and Seino, S. (2000). Insulin secretion and differential gene expression in glucose-responsive and -unresponsive MIN6 sublines. Am. J. Physiol. Endocrinol. Metab. *279*, E773-81.

Miyake, M., Nomura, A., Ogura, A., Takehana, K., Kitahara, Y., Takahara, K., Tsugawa, K., Miyamoto, C., Miura, N., Sato, R., et al. (2016). Skeletal muscle-specific eukaryotic translation initiation factor 2α phosphorylation controls amino acid metabolism and fibroblast growth factor 21-mediated non-cell-autonomous energy metabolism. FASEB J. *30*, 798–812.

Mori, K. (2000). Tripartite management of unfolded proteins in the endoplasmic reticulum. Cell *101*, 451–454.

Nadanaka, S., Okada, T., Yoshida, H., and Mori, K. (2007). Role of disulfide bridges formed in the luminal domain of ATF6 in sensing endoplasmic reticulum stress. Mol. Cell. Biol. *27*, 1027–1043.

Nozaki, J.I., Kubota, H., Yoshida, H., Naitoh, M., Goji, J., Yoshinaga, T., Mori, K., Koizumi, A., and Nagata, K. (2004). The endoplasmic reticulum stress response is stimulated through the continuous

867 activation of transcription factors ATF6 and XBP1 in Ins2+/Akita pancreatic beta cells. Genes Cells *9*,
868 261–270.

869 Oka, O.B., van Lith, M., Rudolf, J., Tungkum, W., Pringle, M.A., and Bulleid, N.J. (2019). ERp18
870 regulates activation of ATF6α during unfolded protein response. EMBO J. *38*, e100990.

871 Oyadomari, S., Koizumi, A., Takeda, K., Gotoh, T., Akira, S., Araki, E., and Mori, M. (2002). Targeted
872 disruption of the Chop gene delays endoplasmic reticulum stress–mediated diabetes. J. Clin. Invest. *109*,
873 525–532.

874 Ozcan, U., Yilmaz, E., Ozcan, L., Furuhashi, M., Vaillancourt, E., Smith, R.O., Görgün, C.Z., and
875 Hotamisligil, G.S. (2006). Chemical chaperones reduce ER stress and restore glucose homeostasis in a
876 mouse model of type 2 diabetes. Science *313*, 1137–1140.

877 Pobre, K.F.R., Poet, G.J., and Hendershot, L.M. (2019). The endoplasmic reticulum (ER) chaperone BiP
878 is a master regulator of ER functions: Getting by with a little help from ERdj friends. J. Biol. Chem. *294*,
879 2098–2108.

880 Preissler, S., Chambers, J.E., Crespillo-Casado, A., Avezov, E., Miranda, E., Perez, J., Hendershot, L.M.,
881 Harding, H.P., and Ron, D. (2015a). Physiological modulation of BiP activity by trans-protomer
882 engagement of the interdomain linker. Elife *4*.

883 Preissler, S., Rato, C., Chen, R., Antrobus, R., Ding, S., Fearnley, I.M., and Ron, D. (2015b). AMPylation
884 matches BiP activity to client protein load in the endoplasmic reticulum. Elife *4*, e12621.

885 Rabhi, N., Salas, E., Froguel, P., and Annicotte, J.-S. (2014). Role of the unfolded protein response in β
886 cell compensation and failure during diabetes. J. Diabetes Res. *2014*, 795171.

887 Rosam, M., Krader, D., Nickels, C., Hochmair, J., Back, K.C., Agam, G., Barth, A., Zeymer, C., Hendrix,
888 J., Schneider, M., et al. (2018). Bap (Sil1) regulates the molecular chaperone BiP by coupling release of
889 nucleotide and substrate. Nat. Struct. Mol. Biol. *25*, 90–100.

Saio, T., Guan, X., Rossi, P., Economou, A., and Kalodimos, C.G. (2014). Structural basis for protein antiaggregation activity of the trigger factor chaperone. Science *344*, 1250494.

Saio, T., Kawagoe, S., Ishimori, K., and Kalodimos, C.G. (2018). Oligomerization of a molecular chaperone modulates its activity. Elife *7*.

Sekine, Y., Zyryanova, A., Crespillo-Casado, A., Amin-Wetzel, N., Harding, H.P., and Ron, D. (2016). Paradoxical sensitivity to an integrated stress response blocking mutation in vanishing white matter cells. PLoS One *11*, e0166278.

Tsuchiya, Y., Saito, M., Kadokura, H., Miyazaki, J.-I., Tashiro, F., Imagawa, Y., Iwawaki, T., and Kohno, K. (2018). IRE1–XBP1 pathway regulates oxidative proinsulin folding in pancreatic β cells. J. Cell Biol. *217*, 1287–1301.

Walter, P., and Ron, D. (2011). The Unfolded Protein Response: From Stress Pathway to Homeostatic Regulation. Science *334*, 1081–1086.

Wang, J., Takeuchi, T., Tanaka, S., Kubo, S.K., Kayo, T., Lu, D., Takata, K., Koizumi, A., and Izumi, T. (1999). A mutation in the insulin 2 gene induces diabetes with severe pancreatic beta-cell dysfunction in the Mody mouse. J. Clin. Invest. *103*, 27–37.

Wieteska, L., Shahidi, S., and Zhuravleva, A. (2017). Allosteric fine-tuning of the conformational equilibrium poises the chaperone BiP for post-translational regulation. Elife *6*.

Xiao, C., Giacca, A., and Lewis, G.F. (2011). Sodium phenylbutyrate, a drug with known capacity to reduce endoplasmic reticulum stress, partially alleviates lipid-induced insulin resistance and beta-cell dysfunction in humans. Diabetes *60*, 918–924.

Yarravarapu, N., Geffert, L., Surratt, C.K., Cascio, M., and Lapinsky, D.J. (2018). Clickable photoaffinity ligands for the human serotonin transporter based on the selective serotonin reuptake inhibitor (S)-citalopram. Bioorg. Med. Chem. Lett. *28*, 3431–3435.

913 Yoshida, H., Haze, K., Yanagi, H., Yura, T., and Mori, K. (1998). Identification of the cis-acting
914 endoplasmic reticulum stress response element responsible for transcriptional induction of mammalian
915 glucose-regulated proteins. Involvement of basic leucine zipper transcription factors. J. Biol. Chem. *273*,
916 33741–33749.

917 Yoshida, H., Matsui, T., Yamamoto, A., Okada, T., and Mori, K. (2001). XBP1 mRNA is induced by
918 ATF6 and spliced by IRE1 in response to ER stress to produce a highly active transcription factor. Cell
919 *107*, 881–891.

920 Yoshida, Y., Sakakura, Y., Aso, N., Okada, S., and Tanabe, Y. (1999). Practical and efficient methods
921 for sulfonylation of alcohols using Ts(Ms)Cl/Et3N and catalytic Me3H·HCl as combined base:
922 Promising alternative to traditional pyridine. Tetrahedron *55*, 2183–2192.

923 Zhang, L., Lai, E., Teodoro, T., and Volchuk, A. (2009). GRP78, but not protein-disulfide isomerase,
924 partially reverses hyperglycemia-induced inhibition of insulin synthesis and secretion in pancreatic
925 {beta}-cells. J. Biol. Chem. *284*, 5289–5298.

926 Zhang, W., Feng, D., Li, Y., Iida, K., McGrath, B., and Cavener, D.R. (2006). PERK EIF2AK3 control
927 of pancreatic beta cell differentiation and proliferation is required for postnatal glucose homeostasis. Cell
928 Metab. *4*, 491–497.

929 Zito, E., Chin, K.-T., Blais, J., Harding, H.P., and Ron, D. (2010). ERO1-beta, a pancreas-specific
930 disulfide oxidase, promotes insulin biogenesis and glucose homeostasis. J. Cell Biol. *188*, 821–832.

931

Figure legends

Figure 1. The small molecule KM04794 inhibits the UPR.

(A) Schematic of UPR signaling.

(B) Relative luciferase activity in C2C12:UPRE cells treated with 0.5 μg/ml Tm and 25 μM PF-429242 (an S1P inhibitor) for 12 h (n = 3).

(C) Relative luciferase activity in C2C12:ERSE cells treated with 0.5 μg/ml Tm and 40 μM 4u8c for 12 h (n = 3).

(D) Relative luciferase activity in MIN6:AARE cells treated with 0.5 μg/ml Tm and 1 μM GSK2606414 (a PERK inhibitor) for 12 h (n = 3).

(E) Chemical structure of KM04794.

(F) Dose-response curve showing the inhibitory effect of KM04794 on luciferase activity induced by 0.5 μg/ml Tm (DMSO = 100%, Tm only = 0%) for 12 h in C2C12:UPRE cells (n = 3).

(G) Dose-response curve showing the inhibitory effect of KM04794 on luciferase activity induced by 0.5 μg/ml Tm (DMSO = 100%, Tm only = 0%) for 12 h in C2C12:ERSE cells (n = 3).

(H) Dose-response curve showing the inhibitory effect of KM04794 on luciferase activity induced by 0.5 μg/ml Tm (DMSO = 100%, Tm only = 0%) for 12 h in MIN6:AARE cells (n = 3).

All data in (B)-(D) and (F)-(D) are presented as the mean ± SD. $^{**}p < 0.01$.

Figure 2. KM04794 inhibited chemical-induced UPR activation

(A) Relative luciferase activity in C2C12:UPRE cells treated with DMSO, 0.5 μg/ml Tm or 0.5 μg/ml Tm and 20 μM KM04794 at the indicated time points (n = 3). The data are shown with respect to a value of 100 in the DMSO group.

(B) Relative luciferase activity in MIN6:AARE cells treated with DMSO, 0.5 μg/ml Tm or 0.5 μg/ml Tm and 20 μM KM04794 at the indicated time points (n = 3). The data are shown with respect to a value of 100 in the DMSO group.

(C) Relative luciferase activity in C2C12:UPRE cells treated with DMSO, 5 nM Tg or 5 nM Tg and 20 μM KM04794 at the indicated time points (n = 3). The data are shown with respect to a value of 100 in the DMSO group.

(D) Relative luciferase activity in MIN6:AARE cells treated with DMSO, 5 nM Tg or 5 nM Tg and 20 μM KM04794 at the indicated time points (n = 3). The data are shown with respect to a value of 100 in the DMSO group.

(E) Immunoblot analysis of the indicated UPR signaling proteins in MIN6m9 cells treated with DMSO, 1 μg/ml Tm, 1 μg/ml Tm, 20 μM KM04794, and 1 μg/ml brefeldin A (Bre) or 1 μg/ml Bre and 20 μM KM04794 for 6 h (n = 3).

(F) RT-qPCR analysis of the indicated UPR target genes in MIN6m9 cells treated with 1 μg/ml Tm or 1 μg/ml Tm and 20 μM KM04794 at the indicated time points (n = 3).

(G) RT-qPCR analysis of the indicated UPR target genes in MIN6m9 cells treated with 1 μg/ml Bre or 1 μg/ml Bre and 20 μM KM04794 at the indicated time points (n = 3).

All data in (A), (B), (C), (D), (F) and (G) are presented as the mean ± SD. *$p < 0.05$, **$p < 0.01$.

Figure 3. KM04794 alleviated ER protein aggregation and cytotoxicity.

(A) Global translation in MIN6m9 cells treated with 20 μM KM04794 for 8 h was assessed by [35S]Met/Cys labeling (n = 3).

(B) BiP content in detergent-insoluble protein aggregates from MEFs treated with DMSO, 1 μg/ml Tm or 1 μg/ml Tm and 20 μM KM04794 for 12 h (n = 3).

(C) Scheme of the survival assay and crystal violet staining of MEFs treated with the indicated compound according to the Materials and Methods. The graph on the right shows the absorbance of stained cell lysates at 595 nm (n = 3).

(D) Relative cell number of MIN6m9 cells treated with DMSO, 0.25 μg/ml Tm or 0.25 μg/ml Tm and 20 μM KM04794 (n = 4).

All data are presented as the mean ± SD. **$p < 0.01$; N.S., not significant.

Figure 4. Insulin-induced misfolding of insulin and ER stress were alleviated by KM04794.

(A) RT-qPCR analysis of a pancreatic β cell line derived from *Akita* mutant mice treated with 20 μM KM04794 for 8 h (n = 3).

(B) RT-qPCR analysis of doxycycline (DOX)-induced *Akita* mutant insulin-expressing MIN6m9 cells treated with DMSO only, 200 ng/ml DOX or 200 ng/ml DOX and 20 μM KM04794 for 12 h ($n = 3$).
(C) Immunoblot analysis under reducing and nonreducing conditions of samples from DOX-induced *Akita* mutant insulin-expressing MIN6m9 cells treated with DMSO only, 200 ng/ml DOX or 200 ng/ml DOX and 20 μM KM04794 for 12 h. The graph on the right shows the quantification of middle-molecular-weight and high molecular weight (MMW and HMW) proinsulin normalized to monomeric insulin ($n = 4$).
All data are presented as the mean ± SD. *$p < 0.05$, **$p < 0.01$.

Figure 5. KM04794 increased insulin secretion and improved the ER stress-induced loss of insulin secretion.
(A-C) Insulin secretion, insulin content and ratio of secreted insulin per total insulin content in MIN6m9 cells treated with 20 μM KM04794 for 8 h, followed by stimulation with the indicated dose of glucose (Glu) ($n = 3$).
(D and E) Insulin secretion and insulin content in pancreatic islets isolated from wild-type mice treated with 20 μM KM04794 for 8 h, followed by stimulation with the indicated dose of glucose (Glu) ($n = 4$).
(F) CHX chase assay showing the insulin content after treatment with 20 μM KM04794 for 6 h. Open and filled circles indicate samples treated with DMSO and 20 μM KM04794, respectively ($n = 4$).
(G) Insulin secretion ratio calculated as the secreted insulin per total insulin content in MIN6m9 cells treated with DMSO, 1 μg/ml Tm or 1 μg/ml Tm and 20 μM KM04794 for 8 h, followed by stimulation with the indicated dose of glucose (Glu) ($n = 4$).
(H) Mature insulin secretion in MIN6m9 cells treated with DMSO, 1 μg/ml Tm or 1 μg/ml Tm and 20 μM KM04794 for 8 h, followed by stimulation with the indicated dose of glucose (Glu) ($n = 5$).
(I) Scheme of the conditioned medium (CM) experiment and immunoblot analysis of P-Akt, Akt and GAPDH in 3T3L1 cells cultured in CM from MIN6m9 treated with the indicated compound. Buffer refers to KRBH buffer. Insulin (10 nM) was used as a positive control. The graph on the right shows the band intensities as determined by immunoblot analysis (n = 4).

(J) Insulin secretion in DOX-induced mutant insulin (C96Y)-expressing MIN6m9 cells treated with DMSO, 200 ng/ml DOX or 200 ng/ml DOX and 20 μM KM04794 for 12 h ($n = 4$).

All data are presented as the mean ± SD. *$p < 0.05$, **$p < 0.01$.

Figure 6. *In vivo* identification of KM04794-binding proteins revealed the accumulation of KM04794 in the ER.

(A) Structure of KM04794-probe and an overview of the chemical pulldown experiment.

(B) Inhibitory effect of the KM04794-probe on luciferase activity (DMSO = 100%, Tm only = 0%) in the MIN6:AARE reporter cell lines ($n = 3$).

(C) Bubble plot of proteins identified by the MS/MS analysis of MIN6m9 cells. The X-axis shows the abundance ratio of robe to Non-probe. The Y-axis shows the abundance ratio of Probe to Probe plus Non-Probe. The size indicates the number of peptide spectrum matches (PSMs). A green circle indicates a putative specific binding partner. A red circle indicates an ER-related protein. A blue circle indicates BiP.

(D) Bubble plot of proteins identified by the MS/MS analysis of MEFs and MIN6m9 cells. The X-axis shows the abundance ratio of Probe to Non-probe in MIN6m9 cells. The Y-axis shows the abundance ratio of Probe to Non-probe in MEF cells. The size indicates the number of peptide spectrum matches (PSMs). A red circle indicates an ER-related protein. A blue circle indicates BiP.

(E) Cellular components enriched in KM04794-binding proteins identified by Gene Ontology analysis.

All data in (B) are presented as the mean ± SD.

Figure 7. BiP mediated the effects of KM04794

(A) Immunoblot analysis of KDEL (recognized BiP) after streptavidin pulldown of photocrosslinked samples treated with 20 μM KM04794-Probe, 100 μM KM04794 (a competitor) or both ($n = 3$).

(B) RT-qPCR analysis of BiP in control (nontarget) and BiP-knockdown MIN6m9 cells treated with DMSO or 20 μM KM04794 for 6 h ($n = 3$).

(C) Insulin secretion in control (nontarget) and BiP-knockdown MIN6m9 cells treated with DMSO or 20 μM KM04794 for 6 h ($n = 3$).

(D) CHX chase assay after 75 min showing the insulin content after treatment with 20 μM KM04794 for 6 h in control (nontarget) and BiP knockdown MIN6m9 cells ($n = 3$).

(E) Immunoblot analysis of BiP, insulin and β-actin after immunoprecipitation of samples treated with DMSO or 20 μM KM04794 (n = 3).

(F) Aggregation of chemically denatured GAPDH containing DMSO, 1 μM BiP, 10 μM KM04794, or 1 μM BiP and 10 μM KM04794.

All data in (B), (C) and (D) are presented as the mean ± SD. *$p < 0.05$, **$p < 0.01$.

Supplementary Information

Supplemental Figure Legends

Figure S1. KM04794 was less toxic under the conditions in this study.

(A) Relative cell number in the indicated reporter cell lines treated with the indicated concentration of KM04794 for 12 h shown by absorbance measured by the WST-8 assay (DMSO = 100%, $n = 3$).

(B) GFP fluorescence in CHO:CHOP-GFP cells treated with 1 μg/ml Tm and/or the indicated dose of KM04794 for 20 h measured by flow cytometry ($n = 3$).

All data are presented as the mean ± SD. $^{**}p < 0.01$.

Figure S2. KM04794 inhibited chemical-induced UPR activation.

(A) Relative luciferase activity in C2C12:UPRE cells treated with DMSO, 1 mM DTT or 1 mM DTT and 20 μM KM04794 at the indicated time points ($n = 3$). The data are shown with respect to a value of 100 in the DMSO group.

(B) Band intensities determined by the immunoblot analysis of the Tm-treated cells described in Figure 2E ($n = 3$).

(C) Band intensities determined by the immunoblot analysis of the Bre-treated cells described in Figure 2E ($n = 3$).

(D) Immunoblot analysis of the indicated UPR signaling proteins in MEFs treated with DMSO, 1 μg/ml Tm or 1 μg/ml Tm and 20 μM KM04794 for the indicated duration ($n = 3$). N.S. refers to a non-specific band.

(E) Immunoblot analysis of the indicated UPR signaling proteins in MIN6m9 cells treated with Tm and 20 μM KM04794, 1 mM 4PBA or 500 μM TUDCA for 6 h ($n = 2$).

All data in (A), (B) and (C) are presented as the mean ± SD. $^{*}p < 0.05$, $^{**}p < 0.01$.

Figure S3. Establishment of controllable insulin overexpressed cells.

(A) RT-qPCR analysis of doxycycline (DOX)-induced wild-type insulin-expressing MIN6m9 cells treated with water or 200 ng/ml DOX for 12 h ($n = 3$).

(B) Immunoblot analysis under reducing and nonreducing conditions of the samples from DOX-induced wild-type or *Akita* mutant insulin-expressing HEK293 cells treated with water or 200 ng/ml DOX for 24 h ($n = 2$). N.S. indicates non-specific bands.

Figure S4. KM04794 increased the insulin content through a posttranscriptional mechanism.

(A) Insulin content in MIN6m9 cells treated with the indicated dose of KM04794 for 8 h ($n = 3$).

(B) Insulin content in MIN6m9 cells treated with 20 μM KM04794, 1 mM 4PBA or 500 μM TUDCA for 8 h ($n = 3$).

(C-D) Insulin secretion and insulin content in MIN6m9 cells treated with 5 μM IBT21 for 8 h, followed by stimulation with the indicated dose of glucose (Glu) ($n = 5$).

(E) RT-qPCR analysis of the *Ins2* gene in MIN6m9 cells treated with 20 μM KM04794 for the indicated duration ($n = 3$).

(F) Insulin content in MIN6m9 cells treated with 20 μM KM04794 and 1 μg/ml actinomycin D for 8 h ($n = 3$).

(G) Proinsulin secretion in MIN6m9 cells treated with DMSO, 1 μg/ml Tm or 1 μg/ml Tm and 20 μM KM04794 for 8 h, followed by stimulation with the indicated dose of glucose (Glu) ($n = 5$).

(H) Ratio of secreted proinsulin molecule per secreted mature insulin molecule in MIN6m9 cells treated with DMSO, 1 μg/ml Tm or 1 μg/ml Tm and 20 μM KM04794 for 8 h, followed by stimulation with the indicated dose of glucose (Glu) ($n = 5$).

All data are presented as the mean ± SD. *$p < 0.05$, **$p < 0.01$; N.S., not significant.

Figure S5. KM04794 accumulated in the ER and directly bound the molecular chaperone BiP.

(A) Inhibitory effect of KM04794-probe on luciferase activity (DMSO = 100%, Tm only = 0%) in C2C12:ERSE reporter cell lines ($n = 3$).

(B) Inhibitory effect of the KM04794 probe on luciferase activity (DMSO = 100%, Tm only = 0%) in C2C12:UPRE reporter cells ($n = 3$).

(C) Visualization of SDS-PAGE results by silver staining after streptavidin pulldown of photocrosslinked samples treated with 20 μM KM04794-probe, 100 μM KM04794 (a competitor) or both ($n = 2$).

(D) Biological components enriched in KM04794-binding proteins determined by Gene Ontology analysis.

All data in (A) and (B) are presented as the mean ± SD.

Figure S6. Identification of proteins mediating the effects of KM04794.

(A) Relative insulin contents (upper) and gene expression levels of target genes (lower) in each guideRNA-expressing MIN6m9:KRAB-dCas9 cell (insulin: n =3, gene expression: n = 2). Cells used to measure insulin contents were treated with 20 μM KM04794 for 8 h. The data are shown as a value of 1 in the nontarget group.

(B) RT-qPCR analysis of the indicated UPR target genes in the control (nontarget) and BiP-knockout MIN6m9 cells treated with DMSO or 20 μM KM04794 for 6 h (n = 3).

(C) Band intensities were determined by immunoblot analysis as described in Figure 7E (n = 3).

(D) Visualization of SDS-PAGE results by Coomassie blue staining of the purified recombinant BiP protein.

(E) Immunoblot analysis using streptavidin-HRP after photocrosslinking between recombinant BiP and KM04794-probe (n = 2).

(F) ATPase activity of recombinant BiP in the presence of the indicated dose of KM04794 (n = 4).

(G) Aggregation of insulin induced by DTT containing the indicated doses of BiP and KM04794. The data are shown with respect to a value of 1 in the no-DTT group and are presented as the mean ± SD.

All data in (A), (B), (C) and (F) are presented as the mean ± SD. *p < 0.05, **p < 0.01; N.S., not significant.

Figure S7. An anti-ATF6α antibody, ATZ-09, could detect the activation state of ATF6α

(A) Detection of exogenously expressed ATF6α by ELISAs. Rat ATF6α-tagged streptavidin binding peptide (SBP) was overexpressed in HEK293T cells. After SBP-ATF6α was immobilized on an avidin-coated plate, the plate was incubated with ATZ-09 (n = 1).

(B) Immunoblot analysis of endogenous rat and human ATF6α in rat insulinoma INS-1 cells and human osteosarcoma U2OS cells treated with or without 1 mM DTT for 1 h using ATZ-09. The black arrow shows full-length ATF6α. The white arrow shows the cleaved N-terminal domain of ATF6α (n = 1). (C) Immunoblot analysis of endogenous mouse ATF6α in wild-type (WT) and *Atf6*$^{-/-}$ MEFs treated with or without 200 nM Tg for 2 h using ATZ-09. The black arrow shows full-length ATF6α. The white arrow shows the cleaved N-terminal domain of ATF6α (n = 2).

Table S1. Mass spectrometry data of the pulldown assay with the KM04794 probe.

Table S2. Oligo DNA sequence used for RT-qPCR and lentiGuide-Puro vector construction.

Figure 1

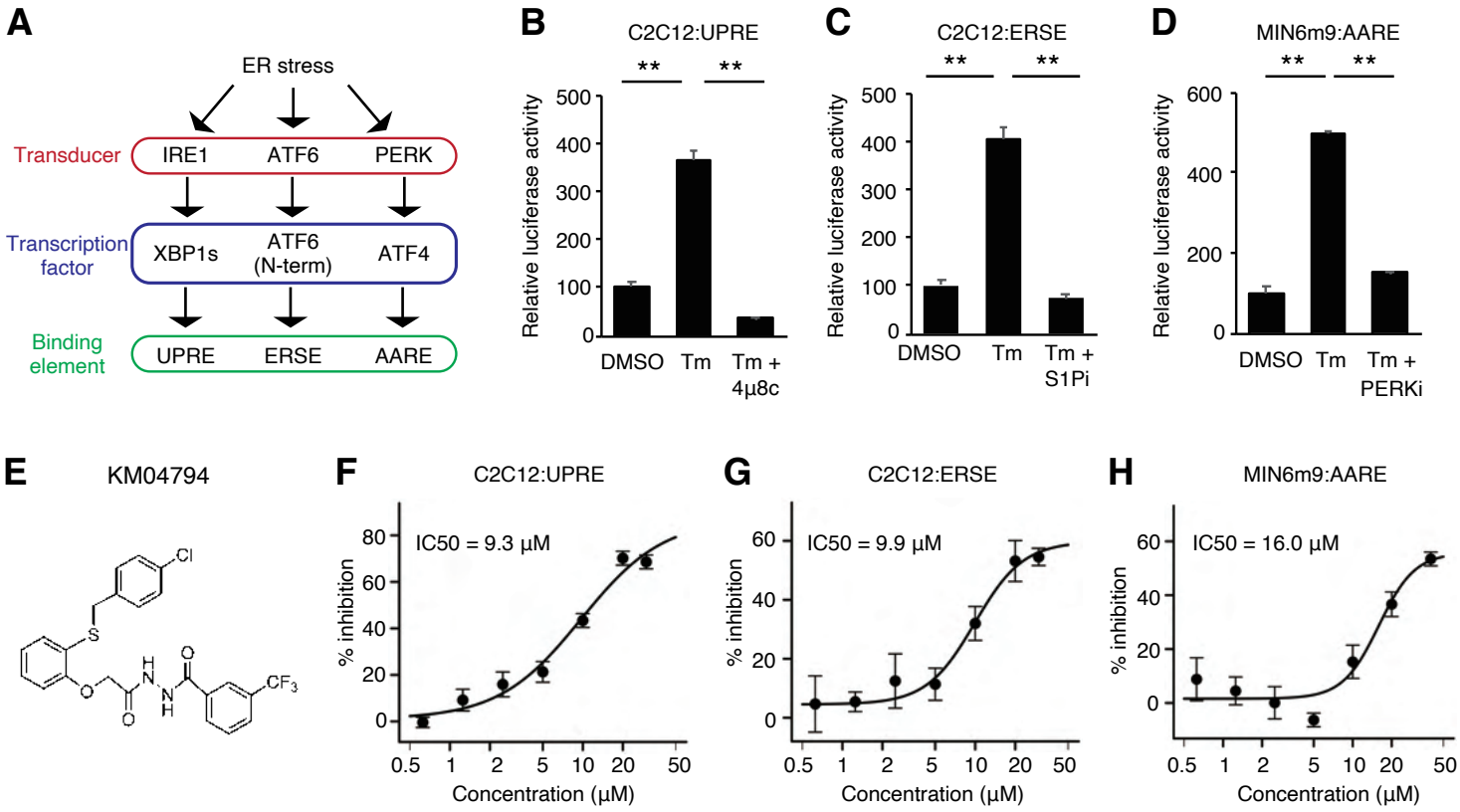
A
ER stress
Transducer
IRE1
ATF6
PERK
Transcription factor
XBP1s
ATF6 (N-term)
ATF4
Binding element
UPRE
ERSE
AARE
B
C2C12:UPRE
Relative luciferase activity
DMSO
Tm
Tm + 4μ8c
C
C2C12:ERSE
Relative luciferase activity
DMSO
Tm
Tm + S1Pi
D
MIN6m9:AARE
Relative luciferase activity
DMSO
Tm
Tm + PERKi
E
KM04794
F
C2C12:UPRE
IC50 = 9.3 μM
% inhibition
Concentration (μM)
G
C2C12:ERSE
IC50 = 9.9 μM
% inhibition
Concentration (μM)
H
MIN6m9:AARE
IC50 = 16.0 μM
% inhibition
Concentration (μM)

Figure 2

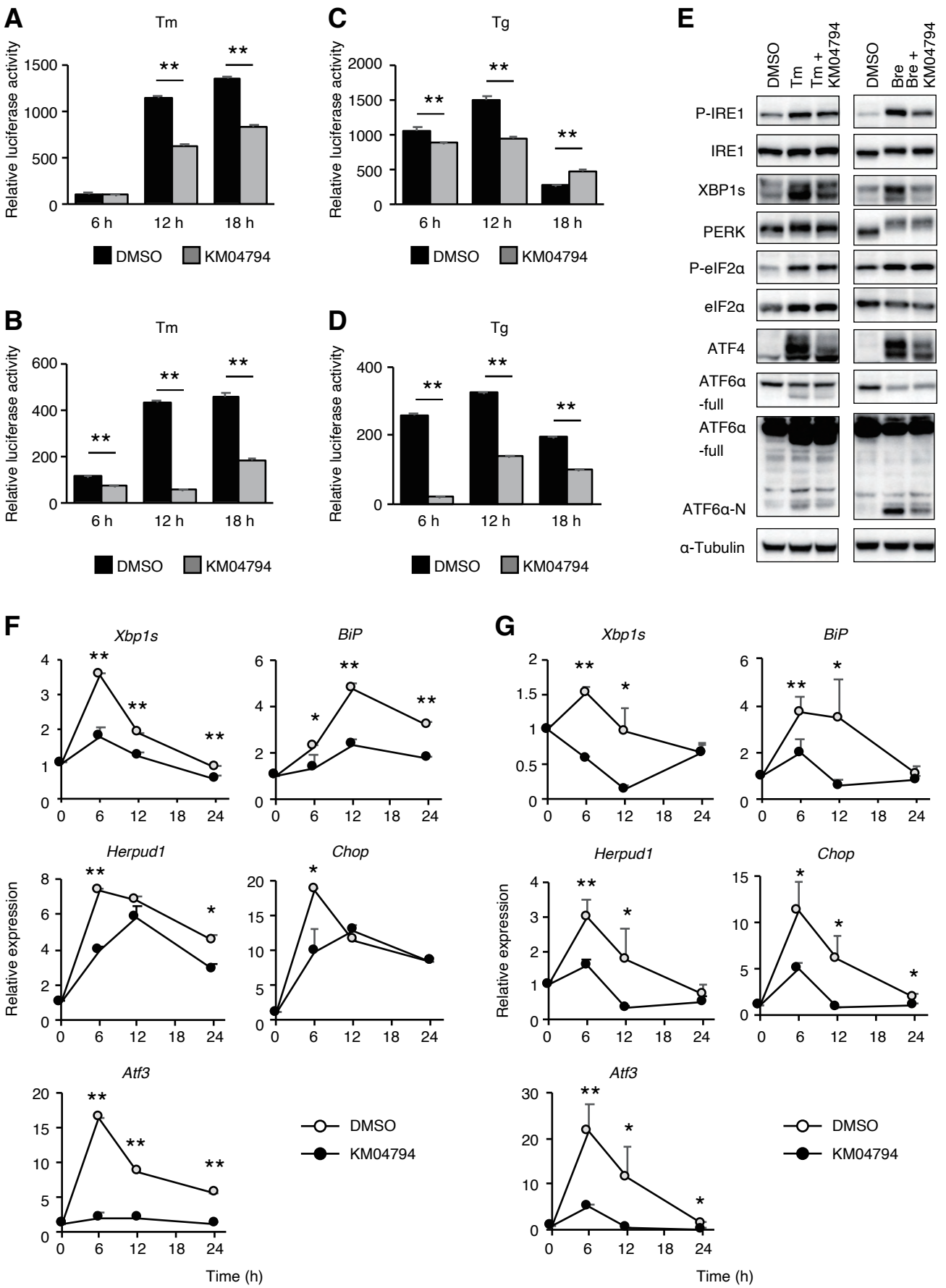
A
Tm
Relative luciferase activity
1500
1000
500
0
6 h
12 h
18 h
DMSO
KM04794
C
Tg
2000
1500
1000
500
0
B
Tm
600
400
200
D
Tg
400
200
E
DMSO
Tm
Tm + KM04794
Bre
Bre + KM04794
P-IRE1
IRE1
XBP1s
PERK
P-eIF2α
eIF2α
ATF4
ATF6α -full
ATF6α -full
ATF6α-N
α-Tubulin
F
G
Xbp1s
BiP
Herpud1
Chop
Atf3
Relative expression
Time (h)

Figure 3

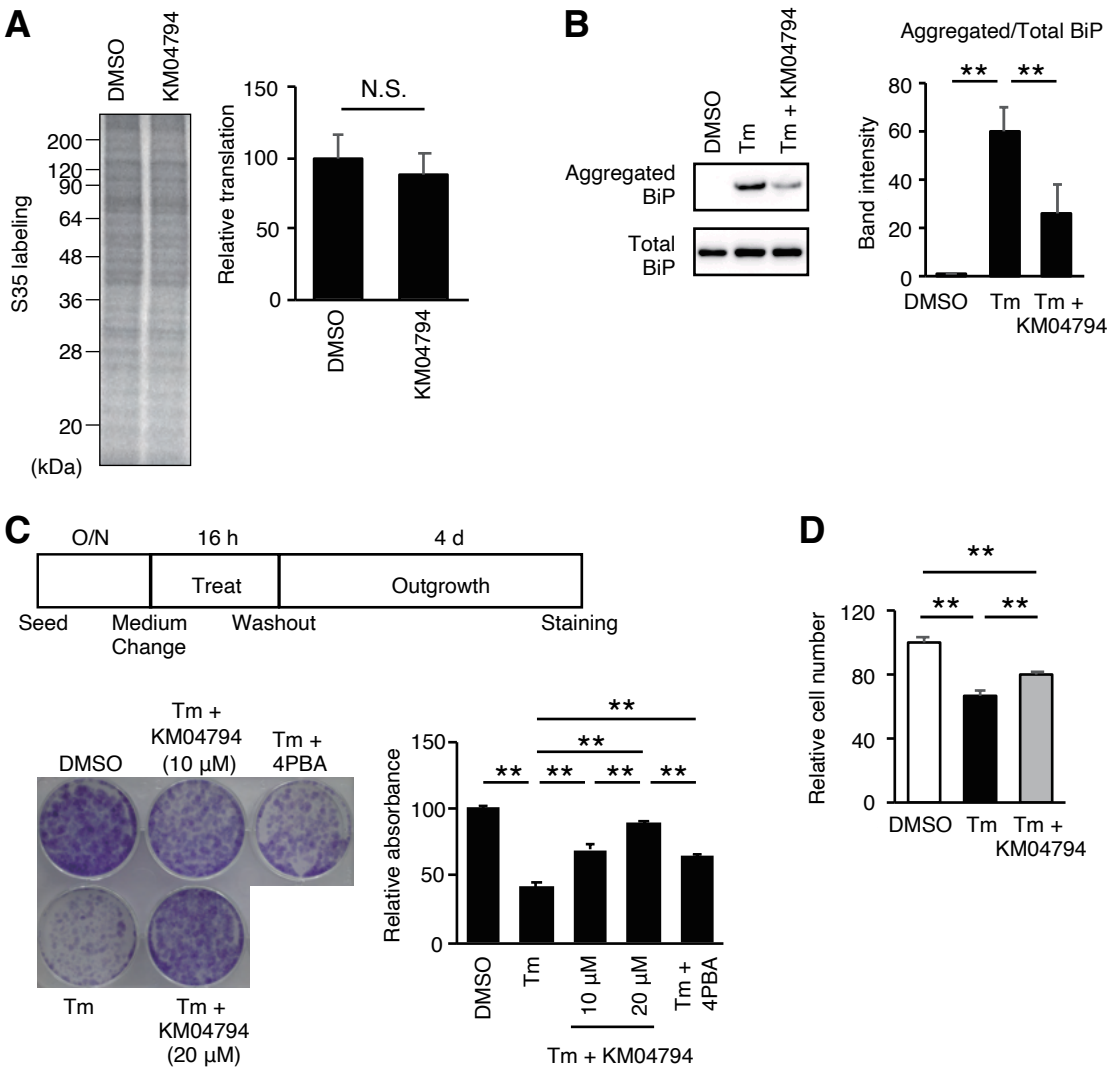
A
DMSO
KM04794
S35 labeling
200
120
90
64
48
36
28
20
(kDa)
Relative translation
150
100
50
0
N.S.
DMSO
KM04794
B
DMSO
Tm
Tm + KM04794
Aggregated BiP
Total BiP
Aggregated/Total BiP
Band intensity
80
60
40
20
0
**
**
DMSO
Tm
Tm + KM04794
C
O/N
16 h
4 d
Treat
Outgrowth
Seed
Medium Change
Washout
Staining
DMSO
Tm + KM04794 (10 μM)
Tm + 4PBA
Tm
Tm + KM04794 (20 μM)
Relative absorbance
150
100
50
0
**
**
**
**
**
DMSO
Tm
10 μM
20 μM
Tm + 4PBA
Tm + KM04794
D
Relative cell number
120
80
40
0
**
**
**
DMSO
Tm
Tm + KM04794

Figure 4

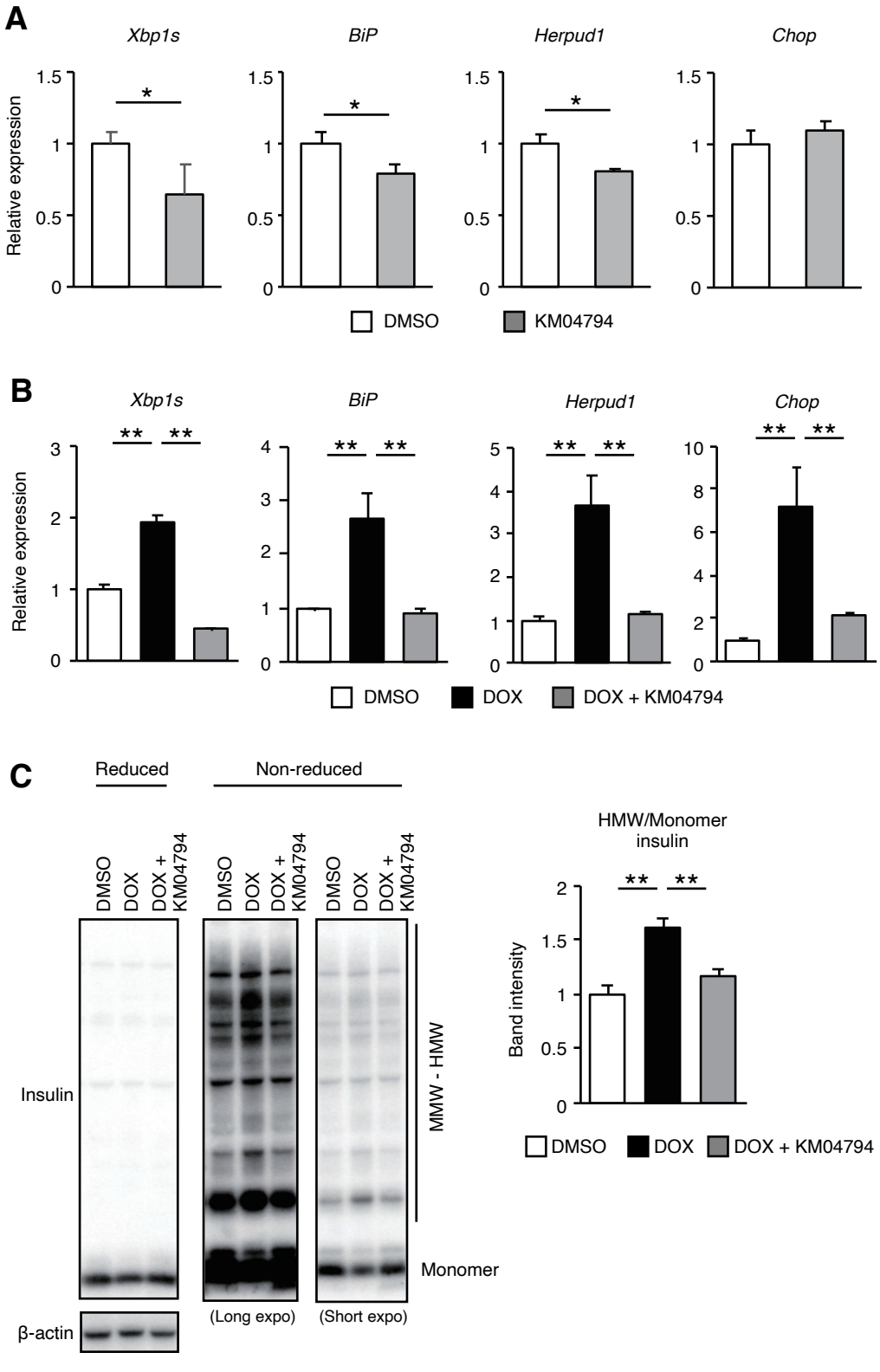
A
Xbp1s
BiP
Herpud1
Chop
Relative expression
DMSO
KM04794
B
Xbp1s
BiP
Herpud1
Chop
Relative expression
DMSO
DOX
DOX + KM04794
C
Reduced
Non-reduced
DMSO
DOX
DOX + KM04794
Insulin
β-actin
(Long expo)
(Short expo)
MMW - HMW
Monomer
HMW/Monomer insulin
Band intensity
DMSO
DOX
DOX + KM04794

Figure5

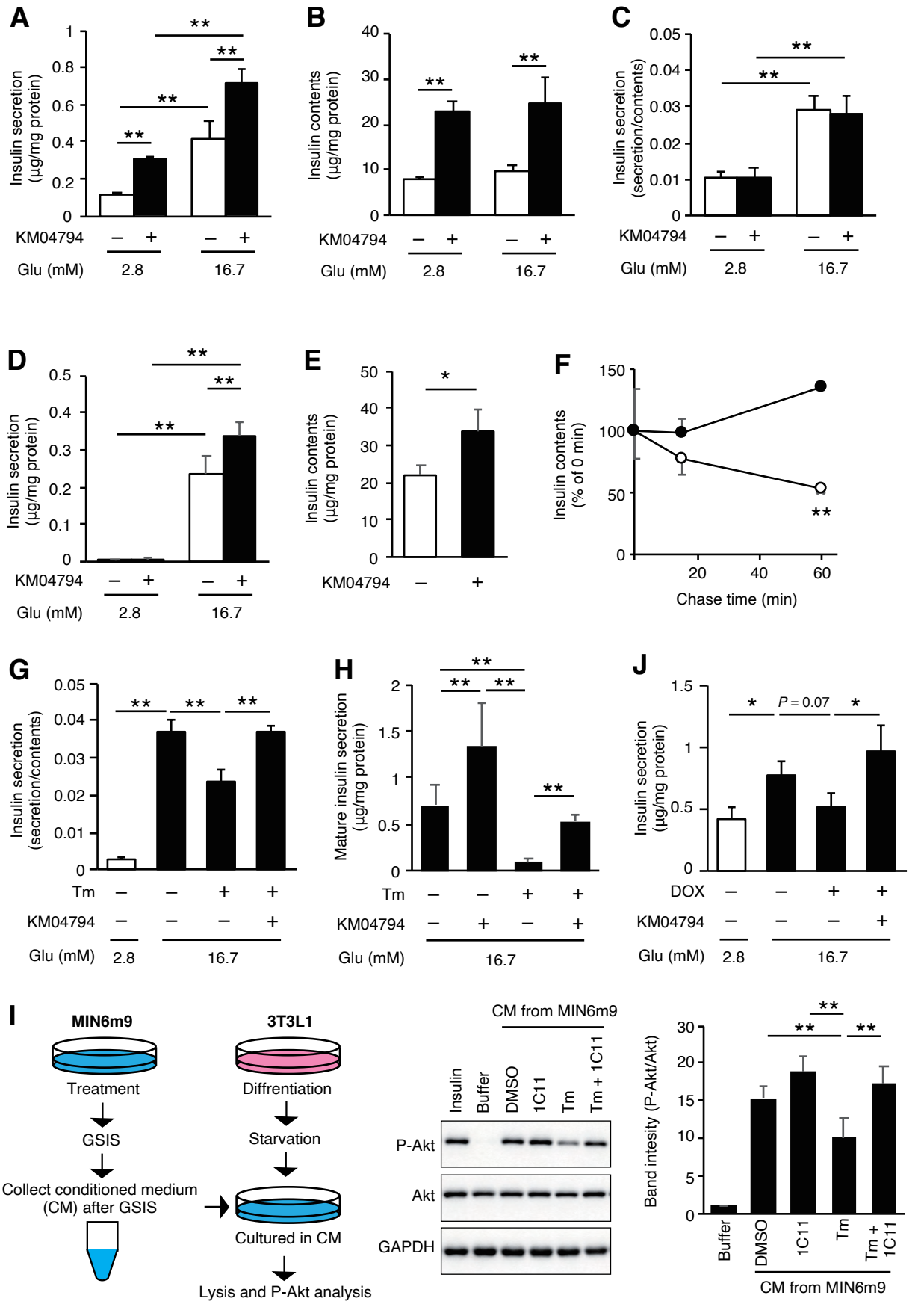
A
Insulin secretion (μg/mg protein)
KM04794
Glu (mM)
2.8
16.7
B
Insulin contents (μg/mg protein)
C
Insulin secretion (secretion/contents)
D
E
F
Insulin contents (% of 0 min)
Chase time (min)
G
Tm
H
Mature insulin secretion (μg/mg protein)
J
DOX
P = 0.07
I
MIN6m9
3T3L1
Treatment
GSIS
Collect conditioned medium (CM) after GSIS
Diffrentiation
Starvation
Cultured in CM
Lysis and P-Akt analysis
CM from MIN6m9
Insulin
Buffer
DMSO
1C11
Tm
Tm + 1C11
P-Akt
Akt
GAPDH
Band intesity (P-Akt/Akt)

Figure 6

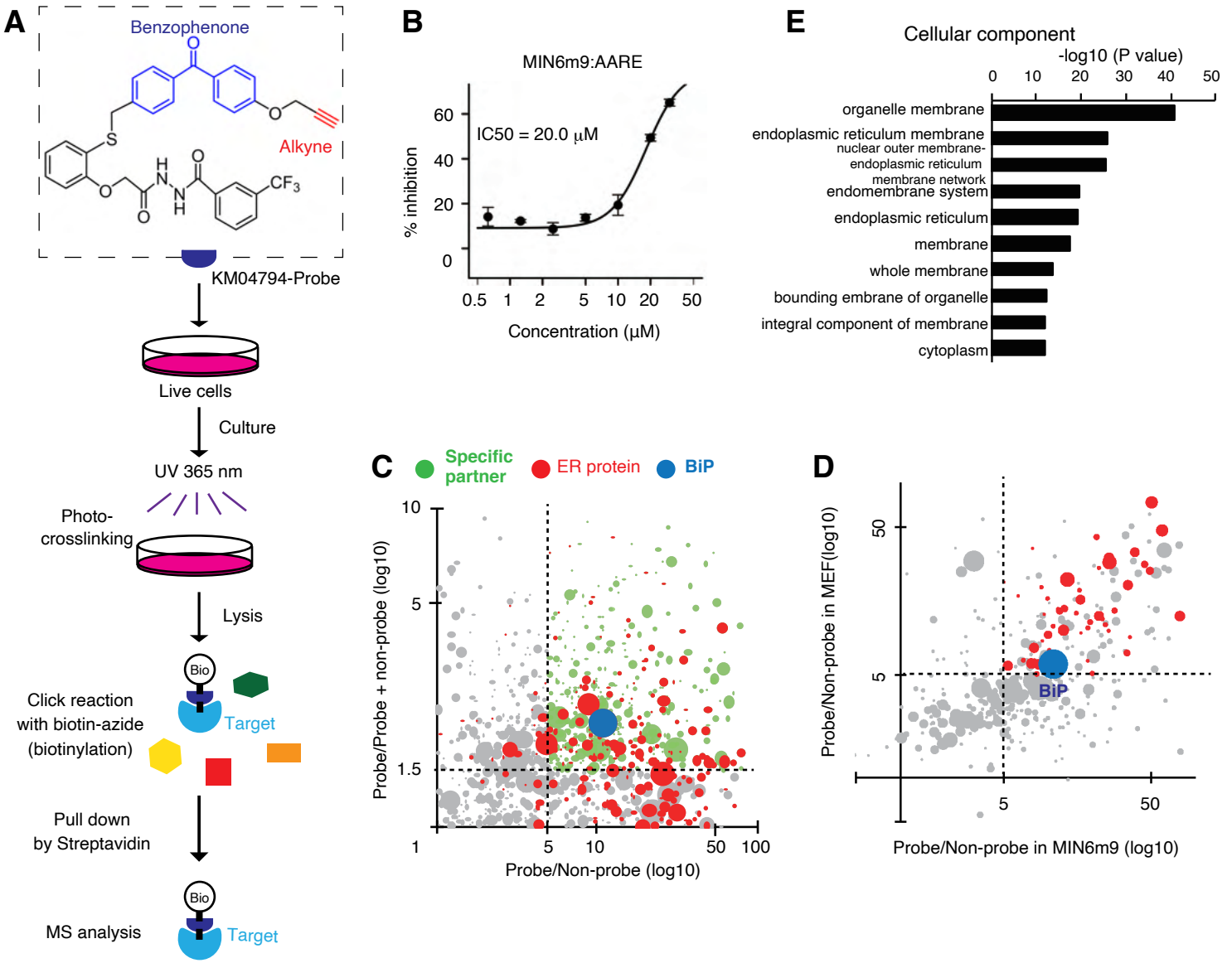
A
Benzophenone
Alkyne
KM04794-Probe
Live cells
Culture
UV 365 nm
Photo-
crosslinking
Lysis
Click reaction
with biotin-azide
(biotinylation)
Bio
Target
Pull down
by Streptavidin
MS analysis
B
MIN6m9:AARE
IC50 = 20.0 μM
% inhibition
Concentration (μM)
C
Specific
partner
ER protein
BiP
Probe/Probe + non-probe (log10)
Probe/Non-probe (log10)
D
Probe/Non-probe in MEF(log10)
Probe/Non-probe in MIN6m9 (log10)
BiP
E
Cellular component
-log10 (P value)
organelle membrane
endoplasmic reticulum membrane
nuclear outer membrane-
endoplasmic reticulum
membrane network
endomembrane system
endoplasmic reticulum
membrane
whole membrane
bounding embrane of organelle
integral component of membrane
cytoplasm

Figure 7

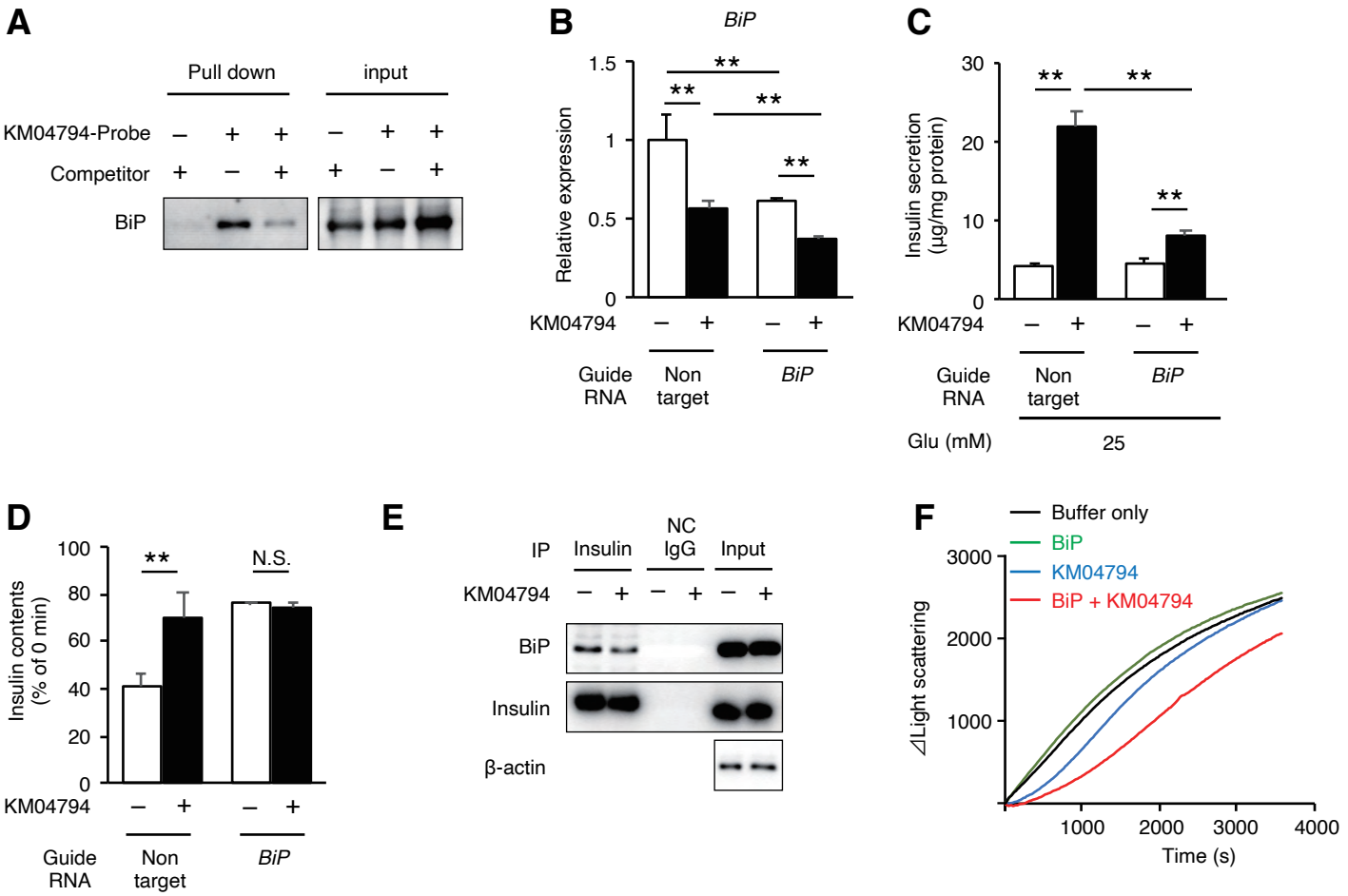
A
Pull down
input
KM04794-Probe
Competitor
BiP
B
BiP
Relative expression
KM04794
Guide RNA
Non target
BiP
C
Insulin secretion (μg/mg protein)
KM04794
Guide RNA
Non target
BiP
Glu (mM)
25
D
Insulin contents (% of 0 min)
N.S.
KM04794
Guide RNA
Non target
BiP
E
IP
Insulin
NC IgG
Input
KM04794
BiP
Insulin
β-actin
F
Buffer only
BiP
KM04794
BiP + KM04794
⊿Light scattering
Time (s)

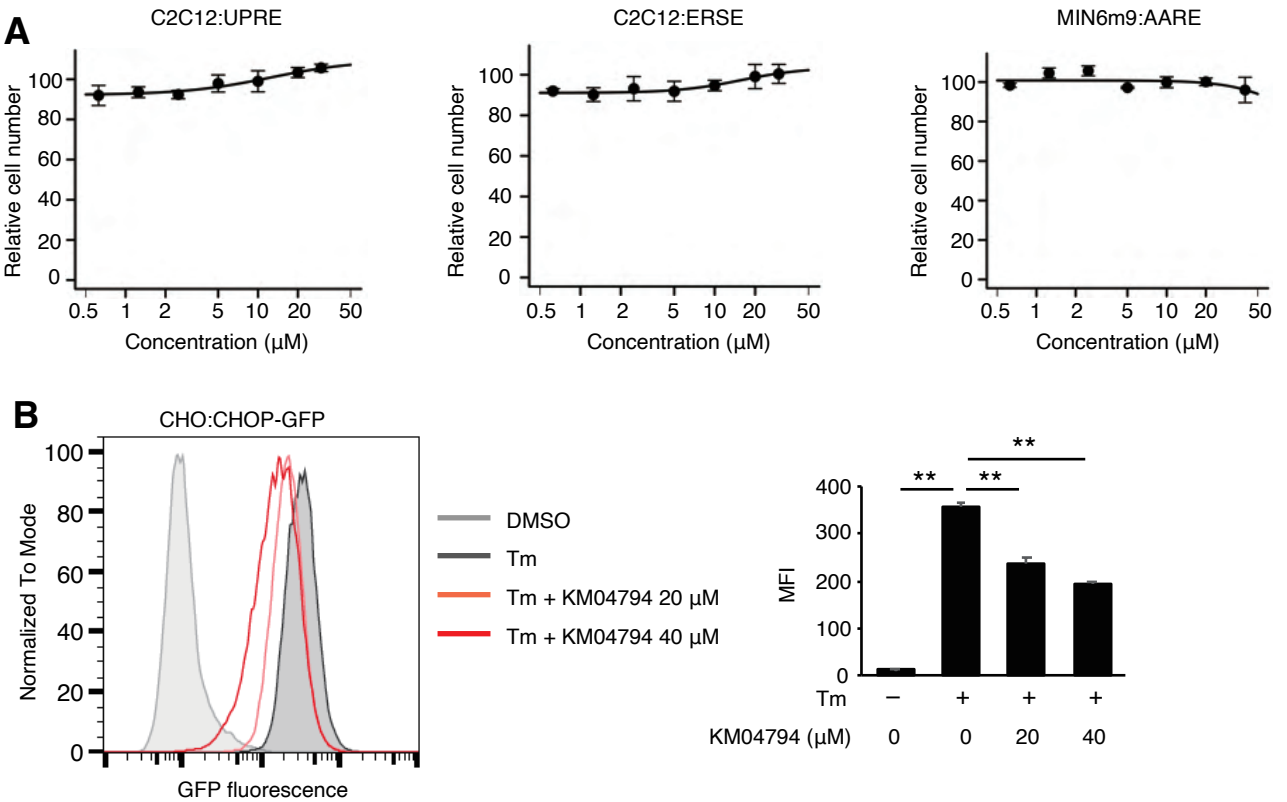

Figure S1. KM04794 was less toxic under the conditions in this study.
(A) Relative cell number in the indicated reporter cell lines treated with the indicated concentration of KM04794 for 12 h shown by absorbance measured by the WST-8 assay (DMSO = 100%, n = 3).
(B) GFP fluorescence in CHO:CHOP-GFP cells treated with 1 μg/ml Tm and/or the indicated dose of KM04794 for 20 h measured by flow cytometry (n = 3).
All data are presented as the mean ± SD. **p < 0.01.

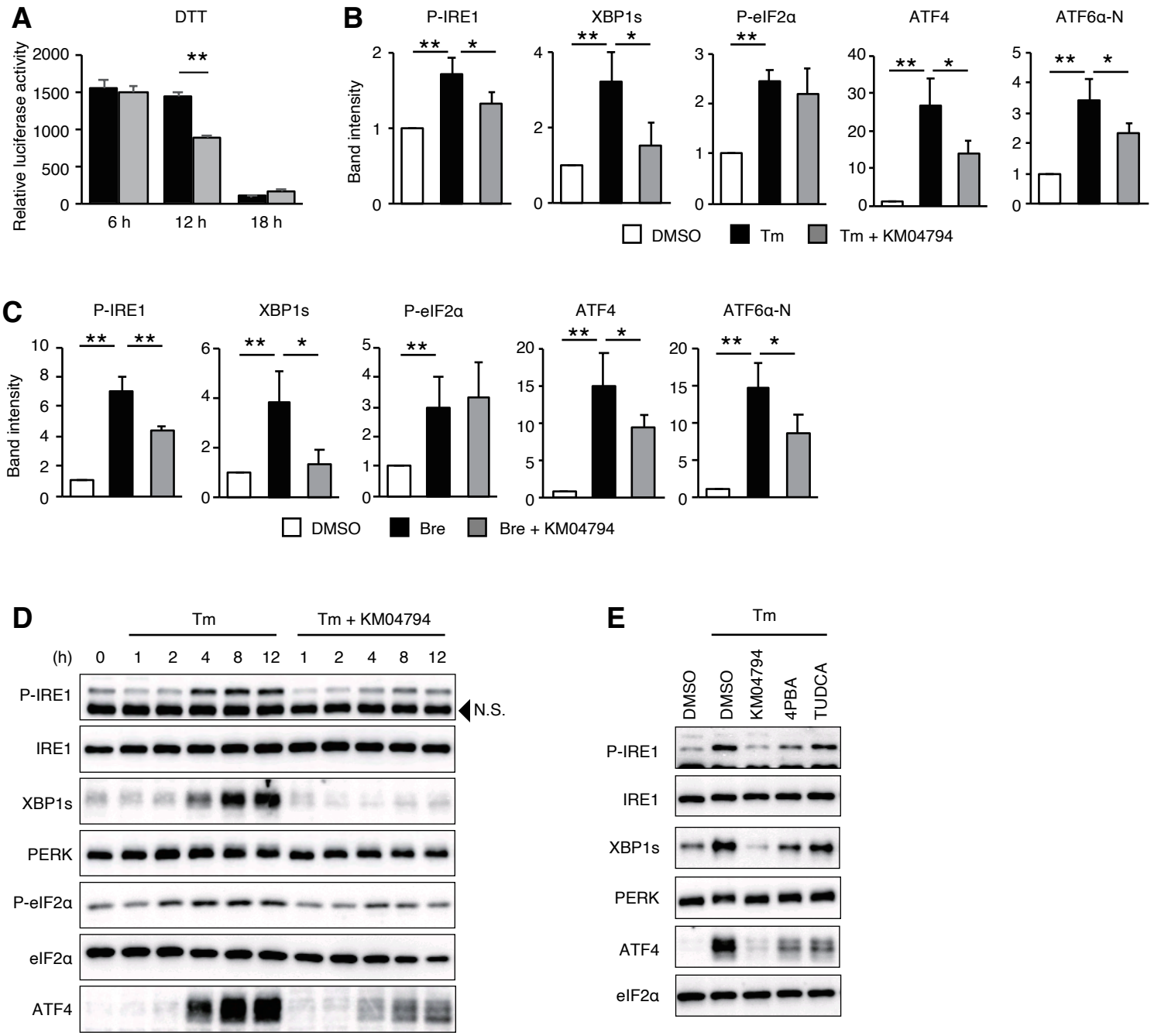

Figure S2. KM04794 inhibited chemical-induced UPR activation.

(A) Relative luciferase activity in C2C12:UPRE cells treated with DMSO, 1 mM DTT or 1 mM DTT and 20 μM KM04794 at the indicated time points (n = 3). The data are shown with respect to a value of 100 in the DMSO group.

(B) Band intensities determined by the immunoblot analysis of the Tm-treated cells described in Figure 2E (n = 3).

(C) Band intensities determined by the immunoblot analysis of the Bre-treated cells described in Figure 2E (n = 3).

(D) Immunoblot analysis of the indicated UPR signaling proteins in MEFs treated with DMSO, 1 μg/ml Tm or 1 μg/ml Tm and 20 μM KM04794 for the indicated duration (n = 3). N.S. refers to a non-specific band.

(E) Immunoblot analysis of the indicated UPR signaling proteins in MIN6m9 cells treated with Tm and 20 μM KM04794, 1 mM 4PBA or 500 μM TUDCA for 6 h (n = 2).

All data in (A), (B) and (C) are presented as the mean ± SD. *$p < 0.05$, **$p < 0.01$.

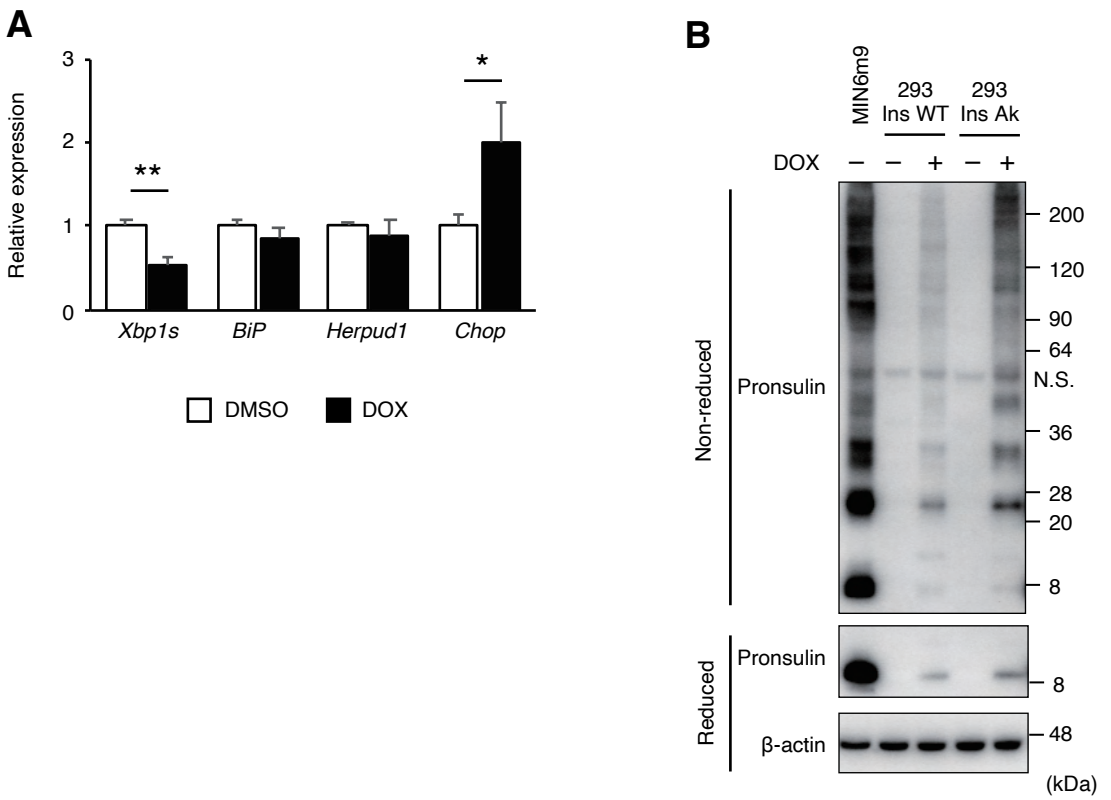

Figure S3. Establishment of controllable insulin overexpressed cells.
(A) RT-qPCR analysis of doxycycline (DOX)-induced wild-type insulin-expressing MIN6m9 cells treated with water or 200 ng/ml DOX for 12 h (n = 3).
(B) Immunoblot analysis under reducing and nonreducing conditions of the samples from DOX-induced wild-type or Akita mutant insulin-expressing HEK293 cells treated with water or 200 ng/ml DOX for 24 h (n = 2). N.S. shows non-specific band.

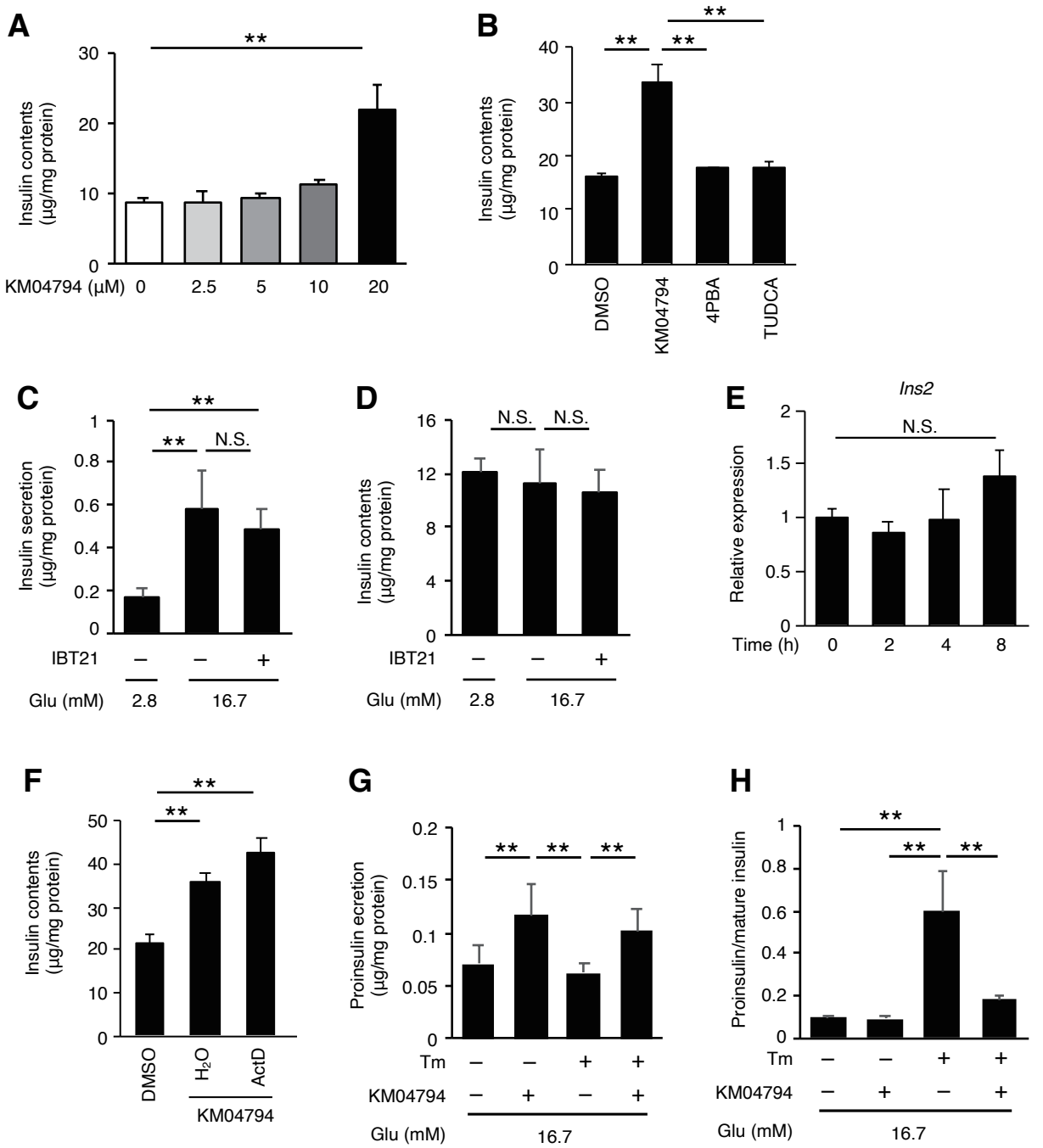

Figure S4. KM04794 increased the insulin content through a posttranscriptional mechanism.

(A) Insulin content in MIN6m9 cells treated with the indicated dose of KM04794 for 8 h (n = 3).

(B) Insulin content in MIN6m9 cells treated with 20 μM KM04794, 1 mM 4PBA or 500 μM TUDCA for 8 h (n = 3).

(C-D) Insulin secretion and insulin content in MIN6m9 cells treated with 5 μM IBT21 for 8 h, followed by stimulation with the indicated dose of glucose (Glu) (n = 5).

(E) RT-qPCR analysis of the Ins2 gene in MIN6m9 cells treated with 20 μM KM04794 for the indicated duration (n = 3).

(F) Insulin content in MIN6m9 cells treated with 20 μM KM04794 and 1 μg/ml actinomycin D for 8 h (n = 3).

(G) Proinsulin secretion in MIN6m9 cells treated with DMSO, 1 μg/ml Tm or 1 μg/ml Tm and 20 μM KM04794 for 8 h, followed by stimulation with the indicated dose of glucose (Glu) (n = 5).

(H) Ratio of secreted proinsulin molecule per secreted mature insulin molecule in MIN6m9 cells treated with DMSO, 1 μg/ml Tm or 1 μg/ml Tm and 20 μM KM04794 for 8 h, followed by stimulation with the indicated dose of glucose (Glu) (n = 5).

All data are presented as the mean ± SD. *$p < 0.05$, **$p < 0.01$; N.S., not significant.

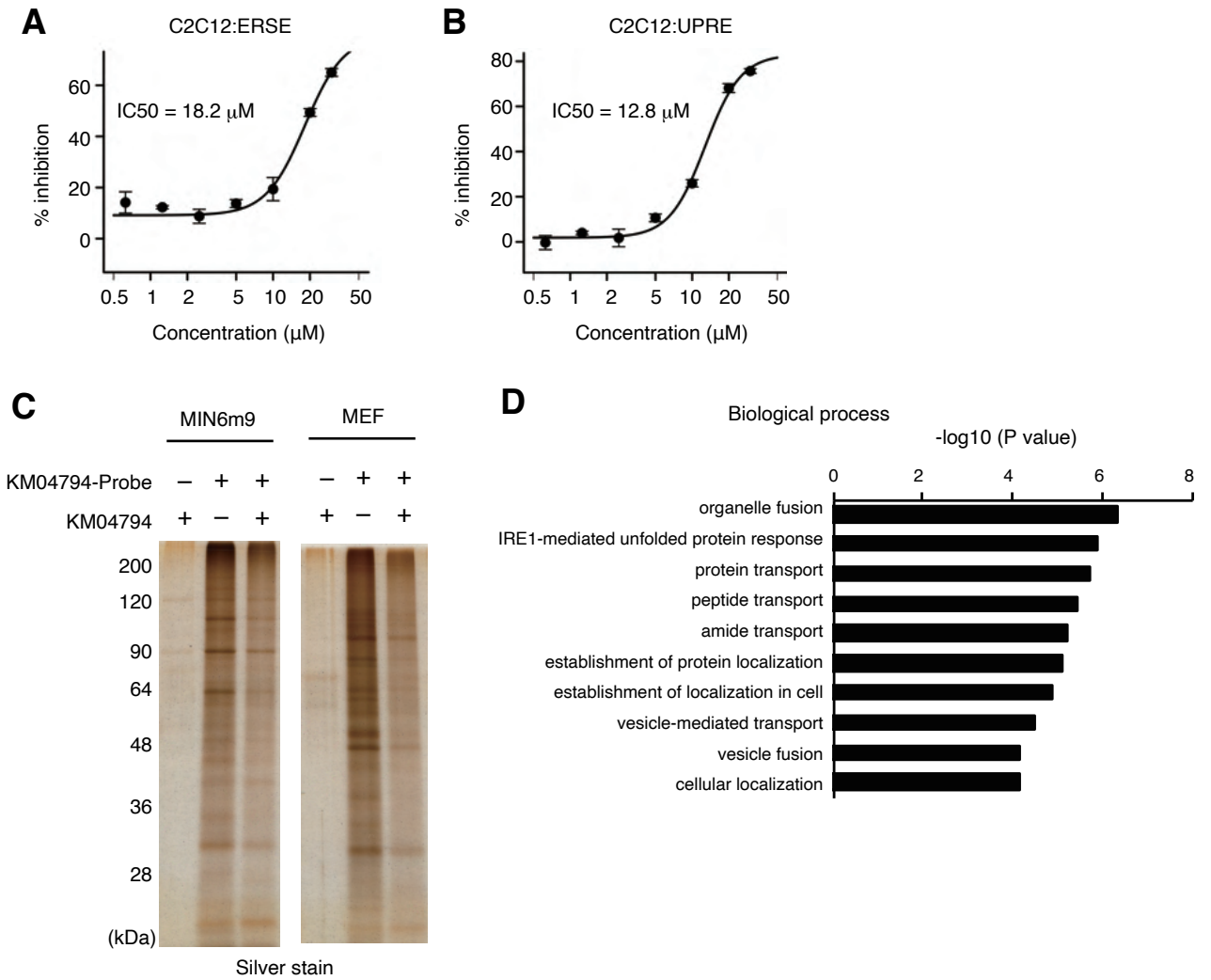

Figure S5. KM04794 accumulated in the ER and directly bound the molecular chaperone BiP.
(A) Inhibitory effect of KM04794-probe on luciferase activity (DMSO = 100%, Tm only = 0%) in C2C12:ERSE reporter cell lines (n = 3).
(B) Inhibitory effect of the KM04794 probe on luciferase activity (DMSO = 100%, Tm only = 0%) in C2C12:UPRE reporter cells (n = 3).
(C) Visualization of SDS-PAGE results by silver staining after streptavidin pulldown of photocrosslinked samples treated with 20 μM KM04794-probe, 100 μM KM04794 (a competitor) or both (n = 2).
(D) Biological components enriched in KM04794-binding proteins determined by Gene Ontology analysis.
All data in (A) and (B) are presented as the mean ± SD.

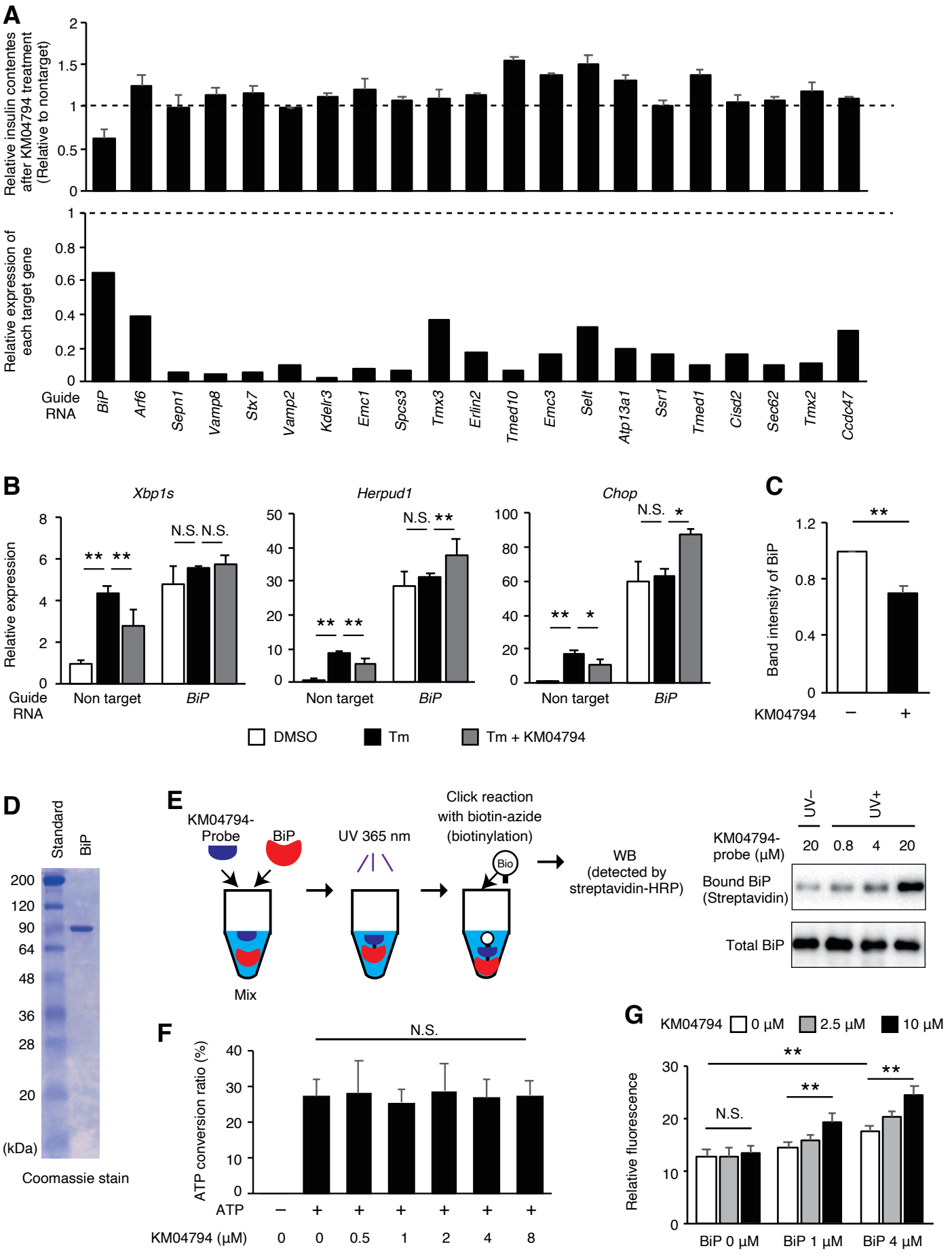
A
Relative insulin contentes after KM04794 treatment (Relative to nontarget)
Relative expression of each target gene
Guide RNA
BiP
Arf6
Sepn1
Vamp8
Stx7
Vamp2
Kdelr3
Emc1
Spcs3
Tmx3
Erlin2
Tmed10
Emc3
Selt
Atp13a1
Ssr1
Tmed1
Cisd2
Sec62
Tmx2
Ccdc47
B
Xbp1s
Herpud1
Chop
Relative expression
Non target
BiP
N.S.
DMSO
Tm
Tm + KM04794
C
Band intensity of BiP
KM04794
D
Standard
BiP
(kDa)
Coomassie stain
E
KM04794-Probe
BiP
UV 365 nm
Click reaction with biotin-azide (biotinylation)
Bio
Mix
WB (detected by streptavidin-HRP)
UV–
UV+
KM04794-probe (μM)
Bound BiP (Streptavidin)
Total BiP
F
ATP conversion ratio (%)
ATP
KM04794 (μM)
G
KM04794
0 μM
2.5 μM
10 μM
Relative fluorescence
BiP 0 μM
BiP 1 μM
BiP 4 μM

Figure S6. Identification of proteins mediating the effects of KM04794.
(A) Relative insulin contents (upper) and gene expression levels of target genes (lower) in each guideRNA-expressing MIN6m9:KRAB-dCas9 cell (insulin: n =3, gene expression: n = 2). The data are shown as a value of 1 in the nontarget group.
(B) RT-qPCR analysis of the indicated UPR target genes in the control (nontarget) and BiP-knockout MIN6m9 cells treated with DMSO or 20 μM KM04794 for 6 h (n = 3).
(C) Band intensities were determined by immunoblot analysis as described in Figure 7E (n = 3).
(D) Visualization of SDS-PAGE results by Coomassie blue staining of the purified recombinant BiP protein.
(E) Immunoblot analysis using streptavidin-HRP after photocrosslinking between recombinant BiP and KM04794-probe (n = 2).
(F) ATPase activity of recombinant BiP in the presence of the indicated dose of KM04794 (n = 4).
(G) Aggregation of insulin induced by DTT containing the indicated doses of BiP and KM04794. The data are shown with respect to a value of 1 in the no-DTT group and are presented as the mean ± SD.
All data in (A), (B), (C) and (F) are presented as the mean ± SD. *$p < 0.05$, **$p < 0.01$; N.S., not significant.

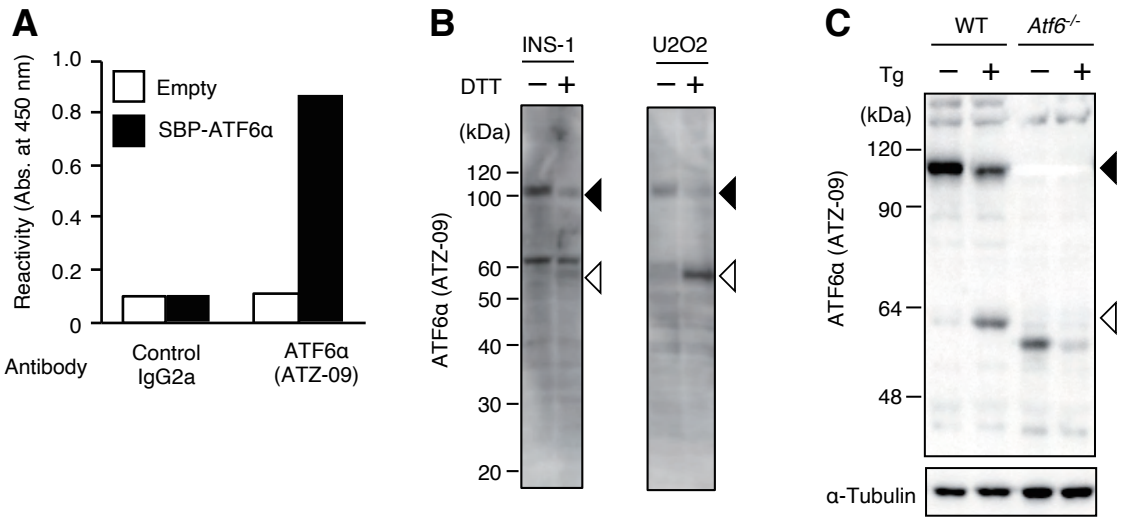

Figure S7. An anti-ATF6α antibody, ATZ-09, could detect the activation state of ATF6α

(A) Detection of exogenously expressed ATF6α by ELISAs. Rat ATF6α-tagged streptavidin binding peptide (SBP) was overexpressed in HEK293T cells. After SBP-ATF6α was immobilized on an avidin-coated plate, the plate was incubated with ATZ-09 (n = 1).

(B) Immunoblot analysis of endogenous rat and human ATF6α in rat insulinoma INS-1 cells and human osteosarcoma U2OS cells treated with or without 1 mM DTT for 1 h using ATZ-09. The black arrow shows full-length ATF6α. The white arrow shows the cleaved N-terminal domain of ATF6α (n = 1).

(C) Immunoblot analysis of endogenous mouse ATF6α in wild-type (WT) and Atf6-/- MEFs treated with or without 200 nM Tg for 2 h using ATZ-09. The black arrow shows full-length ATF6α. The white arrow shows the cleaved N-terminal domain of ATF6α (n = 2).